NATIONAL ADVISORY COMMITTEE FOR AERONAUTICS

TECHNICAL NOTE

No. 1552

INVESTIGATION ON THE VALIDITY OF AN IDEAL THEORY OF ELASTO-PLASTICITY FOR WROUGHT ALUMINUM ALLOYS

By E. G. Thomsen, I. Cornet, I. Lotze,
and J. E. Dorn

University of California

Washington
July 1948

NATIONAL ADVISORY COMMITTEE FOR AERONAUTICS

TECHNICAL NOTE NO. 1552

INVESTIGATION ON THE VALIDITY OF AN IDEAL THEORY OF ELASTO-PLASTICITY FOR WROUGHT ALUMINUM ALLOYS

By E. G. Thomsen, I. Cornet, I. Lotze,
and J. E. Dorn

SUMMARY

The primary purpose of the present investigation was to determine the relation between stresses and plastic strains of wrought aluminum alloys for three types of loading, tension, compression, and torsion. A secondary objective was to identify which assumptions of an ideal theory of elasto-plasticity are invalid for these alloys.

It was found that universal stress-strain curves as predicted by the theory were not obtained with wrought aluminum alloys. The observed disagreement between theory and experiment was attributed to the invalidity of the assumptions of isotropy, constancy of volume, continuity of the metal, and linear stress-infinitesimal plastic strain relations. Fair correlation between the theory and experimental facts, however, was obtained with a cast and solution heat-treated R magnesium alloy which behaved isotropically during plastic deformation. Correlation with some of the aluminum alloys was obtained for the compression and torsion data when shear stresses were plotted as functions of effective strain, but no theoretical justification is available at present for this anomaly.

INTRODUCTION

Theories of plasticity have been the subject of interest for many years. Early investigations were inspired principally by scientific interest in formulating the basic laws of plastic flow. More recently engineers and metallurgists recognized the value of a theory of plasticity for solving practical engineering problems.

St. Venant (reference 1) as early as 1870 conducted investigations under conditions of biaxial stressing which indicated that

$$\frac{P_{\epsilon_{11}}}{\tau_{11} - \frac{1}{2}\tau_{22}} = \frac{P_{\epsilon_{22}}}{\tau_{22} - \frac{1}{2}\tau_{11}} = \frac{P_{\epsilon_{33}}}{-\frac{1}{2}(\tau_{11} + \tau_{22})} \qquad (1)$$

where τ_{11} and τ_{22} are the two principal stresses, and $^{P}\epsilon_{11}$, $^{P}\epsilon_{22}$, and $^{P}\epsilon_{33}$ are the infinitesimal plastic strains in the principal directions. More recent investigations by Lode (reference 2), Taylor and Quinney (reference 3), and others yield experimental results which were in substantial agreement with the dictates of equation (1). Equation (1), however, merely relates the ratios of small strains with the state of stress; additional relations are required to characterize the work-hardened state of the metal. Nadai (reference 4) suggested that if the octahedral shear stress is plotted as a function of the octahedral shear strain, a generalized work-hardening curve is obtained. Prager (reference 5) and also Zener and Hollomon (reference 6) suggested that the invariance of the octahedral shear stress and octahedral shear strain lead to the universality of the curve for all conditions of stress and strain.

During World War II, research on the formability of metals was carried out under the sponsorship of the Office of Scientific Research and Development and the War Production Board of the Office of Production Research and Development. The primary purpose and immediate problem was to obtain empirical data which could be applied to production problems. A second purpose was to develop a theoretical approach to plastic-forming problems so that forming limits could be calculated from simple and easily obtainable data. As a result of these investigations, a formal theory of plasticity was developed (references 7 to 9). It is the purpose of the present investigation to compare the plastic behavior of aluminum alloys under several types of loading with predictions based on this simplified theory.

The authors wish to thank Mr. T. Robinson for his invaluable help in conducting the tests, and they express their appreciation to Messrs. W. F. Pemberton and Muller for their help in preparing specimens for testing. This work was conducted at the University of California under the sponsorship and with the financial assistance of the National Advisory Committee for Aeronautics.

SYMBOLS

ϵ_{ij}, $^{P}\epsilon_{ij}$, $^{E}\epsilon_{ij}$	infinitesimal total, plastic, and elastic strains, respectively
τ_{ij}	true stresses
11, 22, 33	subscripts for principal directions
xx, yy, zz	subscripts for normal stresses and strains on planes of first subscript and in direction of second

xy, yz, zx	subscripts for shear stresses and strains
$^{P}\overline{\phi}$	plastic effective strain
$\overline{\phi}$	total effective strain
$\overline{\sigma}$	effective stress
E	modulus of elasticity
ν	Poisson's ratio
$\overline{\theta}$	hydrostatic tension $\left(\frac{1}{3}\left(\tau_{xx} + \tau_{yy} + \tau_{zz}\right)\right)$
α	stress ratio $\left(\tau_{22}/\tau_{11}\right)$
β	stress ratio $\left(\tau_{33}/\tau_{11}\right)$
L	load
l_0, D_0, A_0	initial gage length, diameter, and area, respectively
l, D, A	instantaneous gage length, diameter, and area, respectively

ELASTO-PLASTICITY THEORY

The theory of elasto-plasticity has been proposed for a material which has the following idealized properties:

(1) The material is continuous

(2) Macroscopic homogeneity

(3) No Bauschinger effect and elastic aftereffect

(4) Time rate phenomena and creep are not present

(5) Macroscopic isotropy

(6) Volume during plastic deformation remains constant

With the assumptions of an ideal material the theory of plasticity requires a stress and a strain analysis. A stress analysis may be made by applying the ordinary laws of mechanics; and a strain analysis, by applying Euclidian geometry. No assumptions other than those contained

in the laws of mechanics and Euclidian geometry are necessary. Two significant invariant quantities result from these analyses, namely:

$$\bar{\sigma} = \sqrt{\frac{\left(\tau_{xx} - \tau_{yy}\right)^2 + \left(\tau_{yy} - \tau_{zz}\right)^2 + \left(\tau_{zz} - \tau_{xx}\right)^2}{2} + 3\left(\tau_{xy}^2 + \tau_{yz}^2 + \tau_{zx}^2\right)} \qquad (2)$$

which is the quadratic deviator stress, and

$$^{P}\bar{\phi} = \int \frac{2}{3}\sqrt{\frac{\left(^{P}\epsilon_{xx} - {}^{P}\epsilon_{yy}\right)^2 + \left(^{P}\epsilon_{yy} - {}^{P}\epsilon_{zz}\right)^2 + \left(^{P}\epsilon_{zz} - {}^{P}\epsilon_{xx}\right)^2}{2} + \frac{3}{4}\left(^{P}\epsilon_{xy}^2 + {}^{P}\epsilon_{yz}^2 + {}^{P}\epsilon_{zx}^2\right)} \qquad (3)$$

which is the quadratic plastic deviator strain. The functions $\bar{\sigma}$ and $^{P}\bar{\phi}$ have been termed the effective stress and effective strain, respectively, and differ by constants only from the octahedral shear stress and octahedral shear strain. For the complete formulation of a theory, it is necessary to establish a relation between the stresses and the infinitesimal strains and the work of plastic deformation. These relations may be obtained by making two assumptions as follows:

(7) The infinitesimal plastic strains are linear functions of the stresses, and the infinitesimal elastic strains are linear functions of the infinitesimal changes in stresses.

(8) The work-hardened state of a metal depends only on the amount of work of plastic deformation and is independent of the stress or strain path employed.

Assumption (7) results in six plasticity equations of the form

$$\left.\begin{aligned}
{}^{P}\epsilon_{xx} &= \frac{3}{2}\frac{d^{P}\bar{\phi}}{\bar{\sigma}}\left(\tau_{xx} - \bar{\theta}\right) \\
{}^{P}\epsilon_{yy} &= \frac{3}{2}\frac{d^{P}\bar{\phi}}{\bar{\sigma}}\left(\tau_{yy} - \bar{\theta}\right) \\
{}^{P}\epsilon_{zz} &= \frac{3}{2}\frac{d^{P}\bar{\phi}}{\bar{\sigma}}\left(\tau_{zz} - \bar{\theta}\right) \\
{}^{P}\epsilon_{xy} &= 3\frac{d^{P}\bar{\phi}}{\bar{\sigma}}\,\tau_{xy} \\
{}^{P}\epsilon_{yz} &= 3\frac{d^{P}\bar{\phi}}{\bar{\sigma}}\,\tau_{yz} \\
{}^{P}\epsilon_{zx} &= 3\frac{d^{P}\bar{\phi}}{\bar{\sigma}}\,\tau_{zx}
\end{aligned}\right\} \tag{4}$$

and assumption (8) leads to the universality of the effective stress–effective plastic strain relation

$$\bar{\sigma} = \bar{\sigma}\left({}^{P}\bar{\phi}\right) \tag{5}$$

If the generalized Hooke's law is introduced by assuming that the elastic properties of the metal are independent of plastic deformation, six elasto-plastic equations result,

$$\left.\begin{aligned}
\epsilon_{xx} &= \frac{3}{2}\frac{d\bar{\phi}}{\bar{\sigma}}\left(\tau_{xx} - \bar{\theta}\right) + \left(\frac{1-2\nu}{E}\right)d\bar{\theta} \\
\epsilon_{yy} &= \frac{3}{2}\frac{d\bar{\phi}}{\bar{\sigma}}\left(\tau_{yy} - \bar{\theta}\right) + \left(\frac{1-2\nu}{E}\right)d\bar{\theta} \\
\epsilon_{zz} &= \frac{3}{2}\frac{d\bar{\phi}}{\bar{\sigma}}\left(\tau_{zz} - \bar{\theta}\right) + \left(\frac{1-2\nu}{E}\right)d\bar{\theta} \\
\epsilon_{xy} &= 3\frac{d\bar{\phi}}{\bar{\sigma}}\,\tau_{xy} \\
\epsilon_{yz} &= 3\frac{d\bar{\phi}}{\bar{\sigma}}\,\tau_{yz} \\
\epsilon_{zx} &= 3\frac{d\bar{\phi}}{\bar{\sigma}}\,\tau_{zx}
\end{aligned}\right\} \tag{6}$$

where ϵ_{xx}, ϵ_{yy}, ϵ_{zz}, ϵ_{xy}, ϵ_{yz}, and ϵ_{zx} are now the total components of strain; $\epsilon_{xx} = {}^{P}\epsilon_{xx} + {}^{E}\epsilon_{xx}$, ..., ..., $\epsilon_{xy} = {}^{P}\epsilon_{xy} + {}^{E}\epsilon_{xy}$, ..., and ...

and

$$\bar{\phi} = {}^{P}\bar{\phi} + \frac{2(1+\nu)}{3E}\bar{\sigma} \tag{7}$$

is the total effective strain or simply effective strain. The relation between effective stress and effective strain is

$$\bar{\sigma} = \bar{\sigma}(\bar{\phi}) \tag{8}$$

and like the $\bar{\sigma} - {}^{P}\bar{\phi}$ curve, it is a universal $\bar{\sigma} - \bar{\phi}$ curve.

Several methods may be employed to check the applicability of the idealized theory of plasticity under special conditions. Lode (reference 2) and later Taylor and Quinney (reference 3) made combined stress studies with tubular specimens of various alloys and plotted their results in terms of

$$\left.\begin{aligned} \nu &= \frac{{}^{P}\epsilon_{22} - \frac{1}{2}\left({}^{P}\epsilon_{11} - {}^{P}\epsilon_{33}\right)}{\frac{1}{2}\left({}^{P}\epsilon_{11} - {}^{P}\epsilon_{33}\right)} \\ \mu &= \frac{\tau_{22} - \frac{1}{2}\left(\tau_{11} - \tau_{33}\right)}{\frac{1}{2}\left(\tau_{11} - \tau_{33}\right)} \end{aligned}\right\} \tag{9}$$

where ${}^{P}\epsilon_{11}$, ${}^{P}\epsilon_{22}$, and ${}^{P}\epsilon_{33}$ are the maximum, intermediate, and minimum infinitesimal principal plastic strains, respectively. If the plasticity equations (4) are rewritten for principal stresses and substituted into equations (9), the linear equation

$$\mu = \nu \tag{10}$$

is obtained. The results of Taylor and Quinney, given in figure 1, illustrate that the agreement between theory and experiment is not perfect. Prager (reference 5) suggested that the deviation from linearity between $\mu = \nu$ may be due to the presence of cubic and higher power terms of stress in the stress–strain relations.

Davis (reference 10) measured the components of finite plastic strains of plastically deformed tubular specimens of mild steel under essentially biaxial stress. The loading was so regulated that approximately constant stress ratios were maintained up to the point of necking. Under these conditions, the directions of principal stresses and strains

remain unaltered throughout the entire deformation. The infinitesimal strain ϵ_{xx} on a fiber in the x-direction at instant t, for example, is also the strain on the fiber which was originally in the x-direction. Thus,

$$ {}^{P}\epsilon_{xx} = \frac{\partial {}^{P}\phi_{xx}}{\partial t}\, dt = d{}^{P}\phi_{xx} \tag{11} $$

For these conditions the six plasticity equations (4) reduce to

$$ \left.\begin{aligned} d{}^{P}\phi_{11} &= \frac{3}{2}\frac{d{}^{P}\bar{\phi}}{\bar{\sigma}}\left(\tau_{11} - \bar{\theta}\right) \\ d{}^{P}\phi_{22} &= \frac{3}{2}\frac{d{}^{P}\bar{\phi}}{\bar{\sigma}}\left(\tau_{22} - \bar{\theta}\right) \\ d{}^{P}\phi_{33} &= \frac{3}{2}\frac{d{}^{P}\bar{\phi}}{\bar{\sigma}}\left(\tau_{33} - \bar{\theta}\right) \end{aligned}\right\} \tag{12} $$

where $d{}^{P}\phi_{11}$, $d{}^{P}\phi_{22}$, and $d{}^{P}\phi_{33}$ are the infinitesimal plastic strains of fibers remaining continuously in the principal directions, denoted by the subscripts 11, 22, and 33. The finite principal strains may be obtained by integration of equations (12),

$$ \left.\begin{aligned} {}^{P}\phi_{11} &= \frac{3}{2}\int_{0}^{{}^{P}\bar{\phi}}\left(\frac{\tau_{11} - \bar{\theta}}{\bar{\sigma}}\right)d{}^{P}\bar{\phi} \\ {}^{P}\phi_{22} &= \frac{3}{2}\int_{0}^{{}^{P}\bar{\phi}}\left(\frac{\tau_{22} - \bar{\theta}}{\bar{\sigma}}\right)d{}^{P}\bar{\phi} \\ {}^{P}\phi_{33} &= \frac{3}{2}\int_{0}^{{}^{P}\bar{\phi}}\left(\frac{\tau_{33} - \bar{\theta}}{\bar{\sigma}}\right)d{}^{P}\bar{\phi} \end{aligned}\right\} \tag{13} $$

For essentially constant stress ratios as used in the experiments on mild steel by Davis, the following relations were maintained:

$$ \left.\begin{aligned} \frac{\tau_{22}}{\tau_{11}} &\cong \alpha = \text{Constant} \\ \frac{\tau_{33}}{\tau_{11}} &\cong \beta \cong 0 \end{aligned}\right\} \tag{14} $$

Substitution of α and $\beta = 0$ into equation (2) yields

$$\bar{\sigma} = \tau_{11}\sqrt{1 - \alpha + \alpha^2} \tag{15}$$

and therefore the plasticity equations (equations (13)) reduce to

$$\left.\begin{aligned} {}^{P}\phi_{11} &= \frac{\left(1 - \frac{1}{2}\alpha\right)}{\sqrt{1 - \alpha + \alpha^2}}\,{}^{P}\bar{\phi} \\ {}^{P}\phi_{22} &= \frac{\left(\alpha - \frac{1}{2}\right)}{\sqrt{1 - \alpha + \alpha^2}}\,{}^{P}\bar{\phi} \\ {}^{P}\phi_{33} &= \frac{-\frac{1}{2}(\alpha + 1)}{\sqrt{1 - \alpha + \alpha^2}}\,{}^{P}\bar{\phi} \end{aligned}\right\} \tag{16}$$

The effective plastic strain ${}^{P}\bar{\phi}$ is obtained by integration of equation (3), namely,

$${}^{P}\bar{\phi} = \int_0^{{}^{P}\bar{\phi}} d{}^{P}\bar{\phi} = \frac{2}{3}\sqrt{\frac{\left({}^{P}\phi_{11} - {}^{P}\phi_{22}\right)^2 + \left({}^{P}\phi_{22} - {}^{P}\phi_{33}\right)^2 + \left({}^{P}\phi_{33} - {}^{P}\phi_{11}\right)^2}{2}} \tag{17}$$

The amount of plastic work resulting from plastic deformation under conditions that principal stresses result from the applied loads is given by

$$\text{Plastic work} = \int_0^{{}^{P}\phi_{11}} \tau_{11}\, d{}^{P}\phi_{11} + \int_0^{{}^{P}\phi_{22}} \tau_{22}\, d{}^{P}\phi_{22} + \int_0^{{}^{P}\phi_{33}} \tau_{33}\, d{}^{P}\phi_{33} \tag{18}$$

Substitution of $\alpha = \text{Constant}$ and $\beta = 0$ into equation (18) and the conditions given by equations (15) and (16), the plastic work becomes

$$\text{Plastic work} = \int_0^{{}^{P}\bar{\phi}} \left(\frac{\bar{\sigma}}{\sqrt{1 - \alpha + \alpha^2}}\right)\left(\frac{1 - \frac{1}{2}\alpha}{\sqrt{1 - \alpha + \alpha^2}}\right) d{}^{P}\bar{\phi} + \int_0^{{}^{P}\bar{\phi}} \left(\frac{\alpha\bar{\sigma}}{\sqrt{1 - \alpha + \alpha^2}}\right)\left(\frac{\alpha - \frac{1}{2}}{\sqrt{1 - \alpha + \alpha^2}}\right) d{}^{P}\bar{\phi}$$

or

$$\text{Plastic work} = \int_0^{{}^{P}\bar{\phi}} \bar{\sigma}\, d{}^{P}\bar{\phi} \tag{19}$$

The amount of plastic work, therefore, is the area under a $\bar{\sigma} - {}^{P}\bar{\phi}$ curve and only depends on the amount of deformation, that is, ${}^{P}\bar{\phi}$; it is independent of the strain or stress path employed.

When the general plasticity equations and assumption (8) are satisfied, a single $\bar{\sigma} - {}^{P}\bar{\phi}$ curve is obtained for all conditions of stressing. The data of Davis (reference 10) for carefully annealed mild steel replotted in terms of effective stress and effective plastic strain up to values of strain at which local plastic flow or necking occurred are given in figure 2. Small deviations from the universality of the $\bar{\sigma} - {}^{P}\bar{\phi}$ curve were obtained, but in general the agreement of theory and experiment is good.

In the present investigation, the universality of the $\bar{\sigma} - \bar{\phi}$ curve and hence the theory of elasto-plasticity is tested for several aluminum alloys from data obtained for three methods of loading: (a) simple tension, (b) simple compression, and (c) simple torsion. The experimental determination of the $\bar{\sigma} - \bar{\phi}$ curves from each of these tests is given in the appendix.

SPECIMENS AND MATERIALS

The tension specimens were machined from $\frac{7}{8}$-inch round bars to A.S.T.M standard specifications for 2-inch gage length, tensile test bars. The cylindrical compression specimens were 0.500 inch in diameter and 0.500 inch long, having their axes coincident with the axes of the original bars. In order to obtain the same sampling, the specimens were machined to the same diameter as the tension test bars. The torsion specimens are of a special design to fit the twist gage and torsion testing machine employed. The specifications of the torsion test bar are given in figure 3.

The test materials were standard commercial materials in the form of rolled round bars and heat-treated to various conditions. Table 1 gives the 13 aluminum alloys selected and their nominal composition.

TABLE 1

NOMINAL COMPOSITION OF WROUGHT ALUMINUM ALLOYS

Alloy	Percent of alloying elements (aluminum and impurities constitute remainder)					
	Copper	Silicon	Manganese	Magnesium	Chromium	Zinc
2S-O						
3S-O			1.2			
17S-T	4.0			0.5		
24S-O	4.5		.6	1.5		
24S-T	4.5		.6	1.5		
24S-T80	4.5		.6	1.5		
24S-T86	4.5		.6	1.5		
52S-O				2.5	0.25	
61S-O	.25	0.6		1.0	.25	
61S-W	.25	.6		1.0	.25	
61S-T	.25	.6		1.0	.25	
75S-O	1.6		.2	2.5	.03	5.6
75S-T	1.6		.2	2.5	.03	5.6

EXPERIMENTAL EQUIPMENT AND TECHNIQUE

Tension tests were performed in a Baldwin-Southwark 60,000-pound testing machine. The accuracy of this machine was approximately 1 percent in load. The specimens were screwed into self-alining grips to assure axial alinement. The strains were recorded up to the yield strength of the material with a specially designed averaging extensometer. The extensometer had a gage factor of four and was equipped with a Last-Word dial gage with least divisions of 0.0002 inch. Estimating readings of the dial gage to the nearest 0.0001 inch resulted

in strain determinations to an accuracy of 0.000025 inch per inch. Extensometer readings were continued to total strains of approximately 0.00075 inch per inch in order to establish the elastic portion of the stress–strain diagrams. Strains beyond 0.00075 inch per inch were measured with a special dial indicator over the 2-inch gage length to an accuracy of 0.0005 inch per inch. Beyond the maximum load, strains were calculated from measurements of the minimum diameter of the test bar; a hand micrometer accurate to 0.0001 inch was used. Maximum and minimum diameters (diameters of necked section) were measured in directions 90° to each other in order to detect possible anisotropy of the materials. Loads were applied continuously, and loads and strains were measured simultaneously. The rate of extension was approximately 0.003 inch per minute of cross-head speed in the elastic region and 0.010 inch per minute in the plastic region up to deformations resulting in fracture of the test bar. The rate of plastic deformation resulted in a rate of change of $\bar{\phi}$ of approximately 0.010 per minute. The rate of change of $\bar{\phi}$ with respect to time was approximately the same for the three different tests.

The compression tests were performed in a compression fixture installed in a 60,000-pound Baldwin–Southwark testing machine. The compression fixture was constructed from a two-post die set with parallel ground anvils. All compression specimens were lubicated with a mixture of 1 pound of graphite per gallon of steam cylinder oil in order to reduce friction between anvil and specimens. The specimens were compressed in a step-by-step method. The diameters of the deformed specimens were measured in two directions at zero load to yield the minimum and maximum diameters. Fresh lubricant was applied between steps.

The torsion tests were performed in a special torsion testing machine with fixed alinement between driving head and tailstock. A floating tailstock insured the elimination of a net axial load on the torsion specimen. Torques were measured with a calibrated torsion bar, its twist being recorded by lever arm movement and dial gage. The accuracy of torque measurement was approximately 10 inch-pounds. Twists were recorded on a twist gage with a direct reading dial having least division of 0.50°. An additional vernier permitted twist measurements accurate to 1 minute to be recorded. The gage section was 4.125 inches long. The twist gage was equipped with axial measuring surfaces to permit measurement of axial deformation of the test bar at any stage of deformation. All tests were run continuously, and torque and twist were measured simultaneously.

EXPERIMENTAL RESULTS

Figures 4 and 5 show the experimental nominal stresses and loads as functions of the natural strains for tension and compression. The natural strain has been defined in the conventional manner as the

logarithm of the original area divided by the instantaneous area ($\log_e A_0/A$) for tension and as the logarithm of the instantaneous area divided by the original area ($\log_e A/A_0$) for compression. Figure 6 shows the experimental curves for torsion. The data are plotted as torque against twist per unit length of bar. The solid curves of figures 4, 5, and 6 represent the average results of at least two tests for each alloy and loading condition. The experimental points below fracture are given as open circles, squares, and triangles, and the fracture conditions are indicated by solid symbols. The solid symbols representing fracture on the tension diagrams, however, do not necessarily represent the true fracture points but merely the conditions at which separation of the test bars occurred. The three alloys 2S-O, 3S-O, and 52S-O, which show a sharp knee on the tension diagram during the final stages of the test, are known to have fractured prior to separation. This confirmation has been obtained by means of radiographs. Tensile bars of these alloys were pulled in successive steps during necking of the bar to permit radiographing the necked bar. It was observed that fracture occurred in the center of the bars at conditions approximately represented by the discontinuity of the solid tension stress-strain curves. No direct evidence is available for the other alloys, for it was impossible to stop the tension tests during the final stages of necking.

The effective stress-effective strain curves for tension, compression, and torsion, as calculated from the experimental data for the 13 aluminum alloys investigated, are given in figures 7 to 19. The method of calculation for the effective stress-effective strain curves is given in the appendix. Each curve represents average values of $\bar{\sigma}$ and $\bar{\phi}$ as calculated from two or more individual tests. For the tension data two curves are given, a nominal tension curve and a corrected tension curve. The nominal tension curve was obtained under the assumption that during necking the stress is given by the load divided by the instantaneous area in the neck. It is known, however, that necking introduces a state of combined stress and, therefore, the tension stress calculated under the foregoing assumption is in error. Bridgman (reference 11) suggested that the effective stress over the minimum section of the bar is constant and that an approximate true effective stress may be calculated by the equation

$$\bar{\sigma}_{\text{corrected}} = \frac{L/A}{\left(1 + 2\frac{R}{a}\right)\log_e\left(1 + \frac{1}{2}\frac{a}{R}\right)} \qquad (20)$$

where

L applied load

A minimum area in neck

a radius of neck measured at right angles to axis of test bar

R radius of curvature of neck measured parallel to axis of bar

In order to apply equation (20), it was necessary to measure the radius of curvature R for various values of a. These values were obtained from tension bars for each alloy by successive loading and unloading. Between steps, the tension bars were removed from the testing machine, and the radius of curvature was measured in a Bausch and Lomb contour projector with a magnification of 50. The correction as given by equation (20) was then applied to the uncorrected $\bar{\sigma}$ obtained from the average data of continuous tension tests at equal values of effective strain. It may be observed from the several figures that for some alloys, the corrected and uncorrected tension curves deviate from each other before the maximum load is reached (maximum loads are indicated on the uncorrected tension curves by M.L.). This anomaly has not been fully explained but may be caused by the initial taper present in the bar. It was observed that several of the soft aluminum alloys exhibited a gradual taper over the gage section before the maximum load is reached.

Figures 7 to 19 reveal that the $\bar{\sigma} - \bar{\phi}$ curves for each alloy differ for the different methods of stressing. The torsion curve is below the tension and compression curve for all alloys. The slope of the torsion curve for large values of $\bar{\phi}$ in general approaches zero; this indicates that the rate of work-hardening diminishes. For small strains, the compression curves of all alloys except 52S-O and 61S-W are above the tension curves; for 52S-O and 61S-W alloys the order is reversed. For large strains, the slopes of the compression curves in general decrease; for several alloys the compression curves fall below the tension curves. Alloys 24S-T80 and 24S-T86 yield curves in compression, as shown in figures 12 and 13, respectively, having negative slopes in the early stages of plastic deformation; at large strains, the slopes become positive. The Bridgman correction lowers the tension curves but fails to yield coincidence with the torsion or compression curves for all alloys.

It is interesting to note that the stress-strain curves of figure 4 reveal some significant differences between the 24S-T8 series and the remainder of the alloys. All the stress-strain curves, except those for the 24S-T8 alloys, appear to form a homologous series. Those which have higher tensile strength also show correspondingly greater decreases in flow stress with strain beyond the uniform strain. The 24S-T8 alloys, however, exhibit an anomalously great decrease in flow stress with strain beyond the uniform, and, therefore, their curves intersect those belonging to alloys from the homologous series. This effect is more pronounced in the 24S-T86 alloy than in the 24S-T80 alloy, this fact indicating that it may be associated with the degree of prestraining preliminary to the artificial aging

treatment for making the 24S-T8 series. The compression and torsion data recorded in figures 5 and 6, respectively, also reveal that all alloys except the 24S-T80 series form a more or less homologous set.

DISCUSSION

Figures 7 to 19 reveal that the $\bar{\sigma} - \bar{\phi}$ curves for the various aluminum alloys were unique for each method of straining. Inasmuch as the theory of plasticity demands universality of these curves for any particular alloy, it appears that some of the assumptions contained in the theory are incorrect for plastic deformation of the aluminum alloys under consideration. A critical review of the assumptions, therefore, is required to isolate the factors contributing to the observed disagreement between theory and experiment. The assumptions stated previously are considered in detail in the following paragraphs.

(1) The medium is continuous. This assumption is usually made in treating mediums in certain branches of science, such as hydrodynamics. For metals this assumption may not be valid, since microdiscontinuities usually exist, such as dispersion of hard brittle phases in a ductile matrix. Microcracks are another possible type of discontinuities in metals. In the case of aluminum alloys, density changes observed for the 61S-T alloy during plastic deformation may be due to the presence of microcracks.

(2) Macroscopic homogeneity. Metals in general are not microscopically homogeneous, but their elastic and plastic properties are substantially the same when averaged over small regions about each point at identical states of work-hardening. The assumption of macroscopic homogeneity, however, is not completely fulfilled by metals. The formation of Lueder's lines and necking observed in a tension test are examples of nonhomogeneous deformation. No attempt was made to test macroscopic homogeneity in the present investigation.

(3) No Bauschinger effect and elastic aftereffect. Elastic after-effects are small relative to large plastic strains and therefore are not believed to be important in the present study. Since all tests, except one to be discussed later, were conducted without reversal of stressing, the Bauschinger effect was absent in the present study.

(4) Time rate phenomena and creep are not present. At elevated temperatures, rate phenomena assume paramount importance, whereas at lower temperatures the work-hardened state is the more significant factor. Rate effects and time effects (creep) appear to influence the plastic deformation little, if the metal retains the cold-worked state. This is substantially true for aluminum alloys deformed slowly at atmospheric temperatures. Furthermore, an effort was made to maintain approximately the same strain rate in all tests.

(5) Macroscopic isotropy. Macroscopic isotropy is seldom present in real metals. A metal may be isotropic initially but during plastic deformation develops various types of anisotropy depending on the kind of loading and the extent of deformation. Wrought metals exhibit anisotropy because of preferred orientation of grains and mechanical fibering of the various phases present, and they develop additional anisotropic characteristics as the metal is deformed. The assumption of isotropy is possibly the weakest part of the theory. The data obtained for aluminum alloys when tested in compression and tension revealed that anisotropy was present during plastic deformation. Cross sections of the test bars initially round became elliptical in the deformed bar.

In order to test the applicability of the ideal theory to an isotropic material and possibly to isolate anisotropy as a factor contributing to disagreement between theory and experiment, it is necessary to investigate the plastic behavior of isotropic metals. Such metal was available in carefully cast specimens of R magnesium alloy. Tension, compression, and torsion tests were, therefore, made with this alloy in the as-cast and solution heat-treated conditions. Agreement of the $\bar{\sigma} - \bar{\phi}$ curves is fair, as revealed in figures 20 and 21. For example, the deviation in stress at values of $\bar{\phi} = 0.05$ from a mean value for the solution heat-treated alloy is approximately ±3 percent. At greater effective strains the deviation increases. In general, however, the agreement between theory and experiment is fair for the cast and subsequently solution heat-treated R magnesium alloys. Agreement obtained with these alloys, however, does not establish anisotropy as the main factor contributing to the disagreement obtained with aluminum alloys. It is necessary, therefore, to examine the aluminum-alloy data in greater detail. This may be accomplished by analyzing the torsion data.

If a solid circular cylinder is subjected to simple torsion, the deformation may be described by the transformation of a point at r_0, θ_0, and z_0 initially but at instant t at point r, θ, and z, namely,

$$r = r_0$$

$$\theta = \theta_0 + z_0 t$$

$$z = z_0$$

where

r radius of a point initially at r_0

θ angular displacement of point initially at θ_0

z distance of point along coordinate axis initially at point z_0

t extent of deformation; twist in radians per unit length of bar

The transformation as given by equation (21), therefore, describes deformation by angular displacements of points lying in planes perpendicular to the axis of the cylinder. Fibers in a test bar originally alined with the specimen axis suffer deformation by twisting only, and no changes in dimensions of the bar occur. R magnesium alloys, within the accuracy of experimental measurements, are known to follow the foregoing deformation. In the case of the aluminum alloys, however, twisting of axially alined fibers was accompanied by dimensional changes of the test bars. The experimental evidence is presented in figure 22. In order to account for this anomaly, the equations relating stress and strain of the present theory must be reexamined.

The assumed linear relation between stress and infinitesimal plastic strain results in the following six equations:

$$\left.\begin{aligned}
{}^{P}\epsilon_{xx} &= dA_{11}\tau_{xx} + dA_{12}\tau_{yy} + dA_{13}\tau_{zz} + dA_{14}\tau_{xy} + dA_{15}\tau_{yz} + dA_{16}\tau_{zx} \\
{}^{P}\epsilon_{yy} &= dA_{21}\tau_{xx} + dA_{22}\tau_{yy} + \cdots \\
{}^{P}\epsilon_{zz} &= dA_{31}\tau_{xx} + \cdots \\
{}^{P}\epsilon_{xy} &= \cdots \\
{}^{P}\epsilon_{yz} &= \cdots \\
{}^{P}\epsilon_{zx} &= dA_{61}\tau_{xx} + dA_{62}\tau_{yy} + dA_{63}\tau_{zz} + dA_{64}\tau_{xy} + dA_{65}\tau_{yz} + dA_{66}\tau_{zx}
\end{aligned}\right\} \qquad (22)$$

In these equations, the linear relations are characterized by 36 moduli of the form dA_{ij}. The infinitesimal moduli dA_{ij} are parameters analogous to the moduli of elasticity, and they have dimensions of infinitesimal strain divided by stress. For isotropic materials, equations (22) reduce to equations (4). If simple torsion is considered, all stresses of equations (22) vanish except the shear stress τ_{xy}, which is induced by the applied torque. The six plasticity equations, therefore, reduce to

$$\left.\begin{aligned}
{}^{P}\epsilon_{xx} &= dA_{14}\tau_{xy} \\
{}^{P}\epsilon_{yy} &= dA_{24}\tau_{xy} \\
{}^{P}\epsilon_{zz} &= dA_{34}\tau_{xy} \\
{}^{P}\epsilon_{xy} &= dA_{44}\tau_{xy} \\
{}^{P}\epsilon_{yz} &= dA_{54}\tau_{xy} \\
{}^{P}\epsilon_{zx} &= dA_{64}\tau_{xy}
\end{aligned}\right\} \qquad (23)$$

The reported change in length during twisting demands that the modulus dA_{14} exist. Additional studies on reversing the direction of twisting yield the results recorded in figure 23. These data prove that dA_{14} is a complicated function of the previous strain history. Immediately upon reversal of the stress, the magnitude of dA_{14} changes; but as deformation continues in the new direction of twisting, the value of dA_{14} changes magnitude and sign. The incorporation of such facts in any simple theory of plasticity will indeed be difficult.

Figure 22 shows that continuous twisting of solid aluminum-alloy bars results in extensions of the bars, the magnitude of which depends on the amount of twist and the kind of alloy. The slopes of the curves give a measure of the anisotropy present at any stage, and the rate of change of the slopes, the change in the anisotropy of the alloys. Slopes which are zero initially indicate zero initial anisotropy of the materials, for example, 3S-O alloy; slopes greater than zero indicate initial anisotropy of the materials, such as 61S-T alloy. A constant slope throughout the test, for example, the curves for 61S-T alloy, indicates constant anisotropy throughout the deformation. A changing slope indicates changing anisotropy of the alloy. Alloy 3S-O accordingly is isotropic initially but develops anisotropic characteristics at large deformations.

(6) Volume during plastic deformation remains constant. It is usually accepted that volume changes during plastic deformation are small. The present theory of plasticity can be modified to incorporate volume changes, but the equations become more complicated. In order to test the applicability of the assumption of constancy of volume, the density of 61S-T alloy was determined for several conditions of deformation. The results are shown in figure 24. The experimental values for the compression curve were obtained with the same test bar at various stages of deformation. The tension values were obtained from three sections of a deformed tension bar; density at the largest $\bar{\phi}$ corresponds to the density of the necked region. For the torsion points, only two values were available, the density of the undeformed bar which was obtained from the grip section and that of the deformed bar from the gage section of the bar. The density value of the deformed torsion bar refers to a $\bar{\phi}$ which corresponds to the outer fiber strain and is not directly comparable with the other test results. Variations of density of the several undeformed test bars, corresponding to the experimental points at $\bar{\phi} = 0$, were small when compared with the density changes observed in the deformed bars. It is evident, therefore, that volume during plastic deformation depends on the extent and kind of deformation. The density measurements, incomplete as they are, indicate that the assumption of constancy of volume may not be realized.

In order to explain the phenomena of density variations during plastic deformation, a microcrack hypothesis may be postulated. Random microcracks present in the initial bar, for example, would tend to enlarge during tensile loading. In compression loading, however, it is possible to visualize a partial closing of these cracks, thus accounting for the observed trends in density with straining. Such differences in density change and their possible association with microcracks may well induce differences in the $\bar{\sigma} - \bar{\phi}$ curves for tension and compression.

(7) The infinitesimal plastic strains are linear functions of the stresses. The assumption of linearity between stress and infinitesimal strain leads to a desirable simplification of the plasticity equations. The observed deviations in the $\bar{\sigma} - \bar{\phi}$ curves of solution heat-treated R magnesium alloys may possibly be due to this oversimplification of natural phenomena. Prager (reference 5) suggested that a power series in stress in the stress-strain relations applied to some experimental combined-stress data gave better agreement than the linear relation. Inasmuch as a linear stress-infinitesimal plastic strain theory leads to desirable simplifications in describing the plastic-flow phenomenon, it should be retained at present until such time as this hypothesis becomes untenable.

It is interesting to note that closer agreement between the torsion and compression data is obtained when shear stresses are plotted as functions of effective strain. The order of relative agreement is shown in table 2.

TABLE 2

RELATIVE AGREEMENT BETWEEN TORSION AND COMPRESSION CURVES OF ALUMINUM ALLOYS IF DATA ARE PLOTTED AS SHEAR STRESS AS A FUNCTION OF EFFECTIVE STRAIN

Good	Fair	Poor
24S-O	2S-O	52S-O
61S-O	3S-O	17S-T
24S-T86	24S-T	61S-W
75S-O	24S-T80	61S-T
		75S-T

The poorest agreement between the shear stress against effective strain for any particular alloy is better, however, than that of the $\bar{\sigma} - \bar{\phi}$ curves. This anomaly cannot be explained at present, as a shear stress theory would lead to a nonsymmetrical theory.

CONCLUSIONS

1. The idealized theory for plastic deformation of work-hardenable metals is fairly valid for some applications. For example, tension, compression, and torsion curves for initially isotropic R magnesium alloys and for 2S-O, 52S-O, and 61S-W alloys are suitably correlated by this theory for strains up to about 0.06.

2. The idealized theory for plastic deformation of work-hardenable metals does not provide an accurate basis for analysis of wrought aluminum alloys. Tension, compression, and torsion data obtained for 13 aluminum alloys do not correlate well with analyses based upon the theory.

3. Anisotropy of plastic deformation, discontinuity of the structure, and density variations with deformation and type of loading probably contribute to failure of the theory.

4. Other factors such as the assumption of linearity between stress and infinitesimal strains may also contribute to failure of the theory.

5. Correlation is obtained between torsion and compression data for a few of the aluminum alloys tested, if the maximum shear stress is plotted as a function of the effective strain. Theoretical justification for this method of correlation, however, has not been established.

6. No general theory is available at present to correlate the plastic flow of metals.

University of California
Berkeley, Calif., March 26, 1947

APPENDIX

CALCULATION OF EFFECTIVE STRESS AND EFFECTIVE STRAIN FROM TENSION, TORSION, AND COMPRESSION DATA OF CIRCULAR SOLID BARS

Tension Test

The effective stress $\bar{\sigma}$ of equation (2) in the text reduces to

$$\bar{\sigma} = \tau_{zz} = \frac{L}{A} = \frac{4L}{\pi D^2} = \frac{4L}{\pi D_{max} D_{min}} \tag{A1}$$

where

τ_{zz} axial true stress

L applied load

A instantaneous area of bar at load L

D instantaneous diameter of bar measured under load L for isotropic deformation

D_{max}, D_{min} maximum and minimum diameters of test bar, respectively, under load L for anisotropic deformation

The effective strain $\bar{\phi}$ is composed of two parts as given by equation (7) of the text

$$\bar{\phi} = {}^{P}\bar{\phi} + \frac{2(1 + \nu)}{3E} \bar{\sigma}$$

and for the case of simple tension reduces to

$$\bar{\phi} = \log_e \left(\frac{P_l}{l_0} \right) + \frac{2(1 + \nu)}{3E} \bar{\sigma} \tag{A2}$$

where

l_0 initial gage length of bar

P_l gage length of deformed bar after removal of load

Inasmuch as extension measurements of the bar up to the maximum load were made under load, it is necessary to introduce l, the gage

length of the bar at load L, into equation (A2). Substituting $l = \left(1 + \frac{\sigma}{E}\right) {}^{P}l$ into equation (A2) results in

$$\bar{\phi} = \log_e \left(\frac{l}{l_0}\right) + \frac{(2\nu - 1)}{3E} \bar{\sigma} \tag{A3}$$

and all quantities are determinable.

Extensions beyond the maximum load are unsuitable for calculating the effective strain, and therefore diameter measurements at the minimum section of the bar were substituted. If D and ${}^{P}D$ are the diameters under load and after release of load, respectively, the relation between D and ${}^{P}D$ is

$$D = \left(1 - \nu \frac{\bar{\sigma}}{E}\right) {}^{P}D \tag{A4}$$

For condition of constancy of volume the plastic effective strain becomes

$${}^{P}\bar{\phi} = \log_e \left(\frac{{}^{P}l}{l}\right) = 2 \log_e \left(\frac{D_0}{{}^{P}D}\right) = \log_e \left(\frac{D_0{}^2}{{}^{P}D_{max} \; {}^{P}D_{min}}\right) \tag{A5}$$

Substituting equations (A4) and (A5) in equation (A2) yields

$$\bar{\phi} = \log_e \left(\frac{D_0{}^2}{D_{max} \; D_{min}}\right) + (2 - \nu) \frac{\bar{\sigma}}{3E} \tag{A6}$$

All quantities for the construction of a $\bar{\sigma} - \bar{\phi}$ curve as given by equations (A1) and (A2) or (A6) are available from measurements.

Compression Test

The effective stress is calculated from the expression

$$\bar{\sigma} = \frac{4L}{\pi {}^{P}D^2} = \frac{4L}{\pi \left({}^{P}D_{max} \; D_{min}\right)} \tag{A7}$$

where L is the load reached just before reducing it to zero and ${}^{P}D$ is the diameter after the load has been released to zero. The quantities L and ${}^{P}D$ are measured in this test for various increments of load. The use of equation (A7) results in a small error of $\bar{\sigma}$ because of neglecting the elastic correction on the cross-sectional

area. The effective strain as given by equation (3) of the text reduces to

$$\bar{\phi} = \log_e \left(\frac{P_{D_{max}} P_{D_{min}}}{D_0^2} \right) + \frac{2(1 + \nu)}{3E} \bar{\sigma} \tag{A8}$$

and all quantities are determinable.

Torsion Test

The effective stress for a solid cylindrical bar loaded in torsion (reference 12) reduces to

$$\bar{\sigma} = \left(\frac{\sqrt{3}}{2\pi R_0^3} \right) \left(t \frac{dT}{dt} + 3T \right) \tag{A9}$$

and the effective strain

$$\bar{\phi} = \frac{R_0}{\sqrt{3}} t \tag{A10}$$

where

R_0 initial radius

t twist in radians per unit gage length

T torque, inch-pounds

The value of $\bar{\sigma}$ of equation (A9) may be readily calculated from a plot of the experimental torque-twist curve.

REFERENCES

1. Saint-Venant, Bârre de: Sur l'établissment des équations des mouvements intérieurs opérés dans les corps solides ductiles au delà des limites on l'élasticité pourrait les ramener à leur premier état. Comptus Rendus, vol. 70, 1870, pp. 473-480; also Jour. des Math. Pures et Appliquées, vol. 16, 1871, pp. 308-316 and 373-382.

2. Lode, W.: Der Einfluss der mittleren Hauptspannung auf das Fliessen der Metalle. Forsch.-Arb. Geb. Ing.-Wes., VDI-Verlag G.M.b.H. (Berlin), Heft 303, 1928.

3. Taylor, G. I., and Quinney, H.: The Plastic Distortion of Metals. Phil. Trans. Roy. Soc. (London), ser. A, vol. 230, Nov. 1931, pp. 323-362.

4. Nádai, A.: Plastic Behavior of Metals in the Strain-Hardening Range. Part I. Jour. Appl. Physics, vol. 8, no. 3, March 1937, pp. 205-213.

5. Prager, W.: Strain Hardening under Combined Stresses. Jour. Appl. Phys., vol. 16, no. 12, Dec. 1945, pp. 837-840.

6. Zener, C., and Hollomon, J. H.: Plastic Flow and Rupture of Metals. Trans. Am. Soc. Metals, vol. 33, 1944, pp. 163-215.

7. Dorn, J. E., and Thomsen, E. G.: The Effect of Combined Stresses on the Ductility of Metals. OSRD No. 3218, Serial No. M-213, War Metallurgy Div., NDRC, Feb. 2, 1944.

8. Dorn, J. E., Jelinek, J. J., and Thomsen, E. G.: Study of the Forming Properties of Aluminum Alloy Sheet at Elevated Temperatures: Plasticity of Metals under General Conditions of Stress. OPRD Rep. No. W-134, Aug. 1944.

9. Jelinek, J. J., Latter, A. J., Thomsen, E. G., and Dorn, J. E.: Plastic Flow of Metals. OPRD Rep. No. W-200, May 1945.

10. Davis, E. A.: Yielding and Fracture of Medium-Carbon Steel under Combined Stress. Jour. Appl. Mech., vol. 12, no. 1, March 1945, pp. A-13 - A-24.

11. Bridgman, P. W.: The Stress Distribution at the Neck of a Tensile Specimen. Trans. Am. Soc. Metals, vol. 32, 1944, p. 553.

12. Nádai, A.: Plasticity. McGraw-Hill Book Co., Inc., 1931.

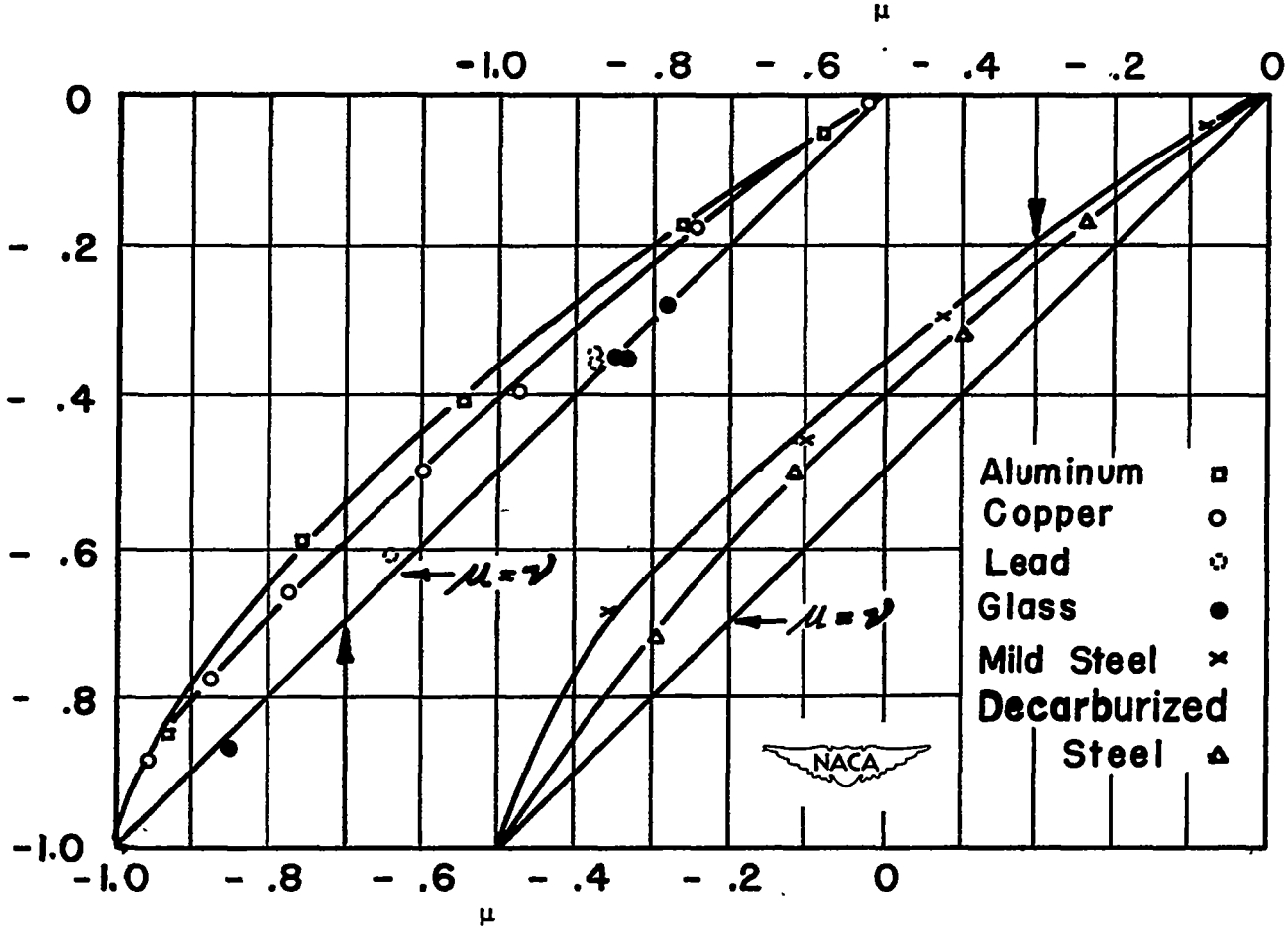

Figure 1.- Combined stress studies by Taylor and Quinney.

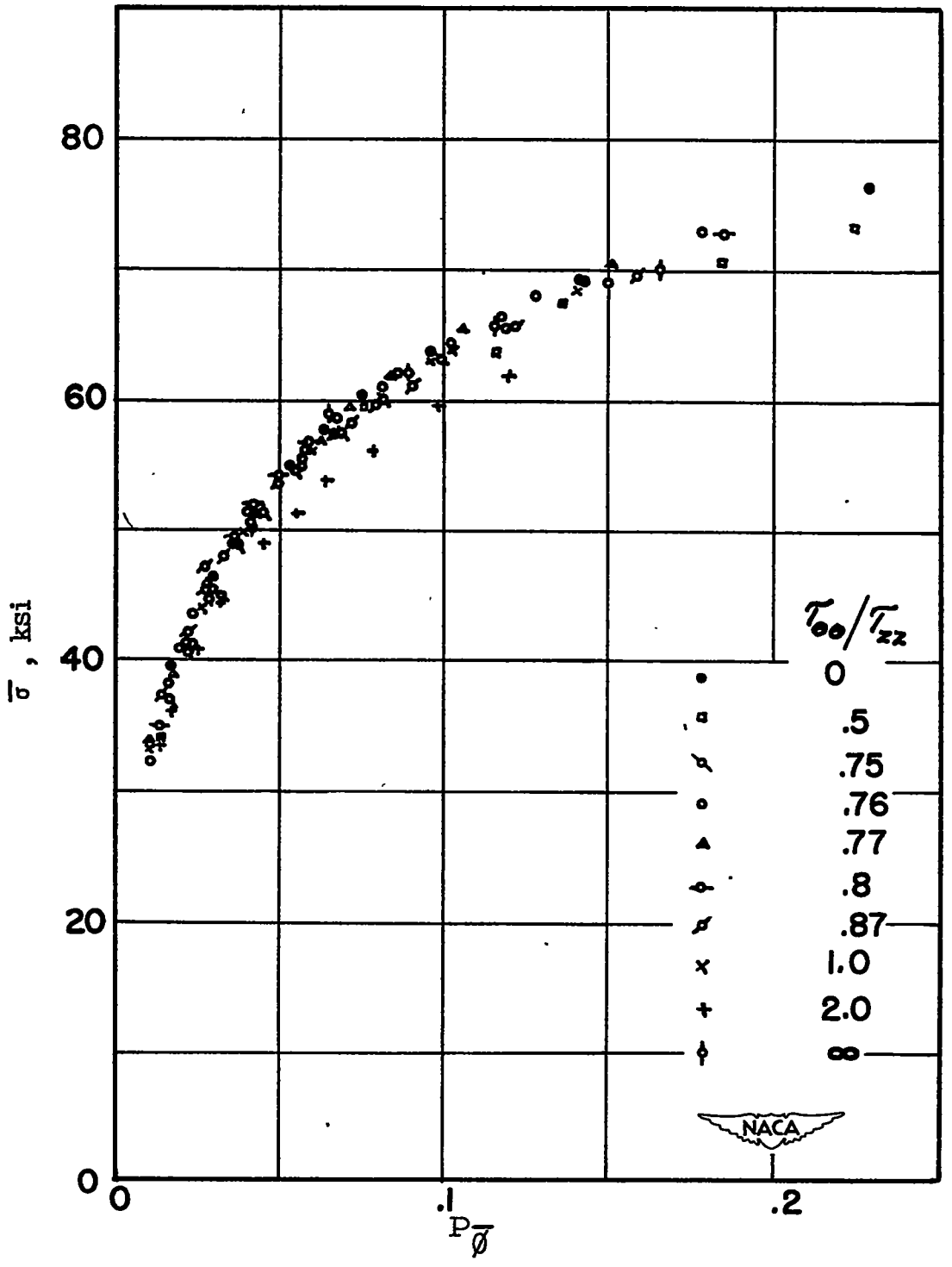

Figure 2.- Combined stress studies with tubular specimens of mild steel by Davis. τ_{zz}, axial stress; $\tau_{\theta\theta}$, hoop stress.

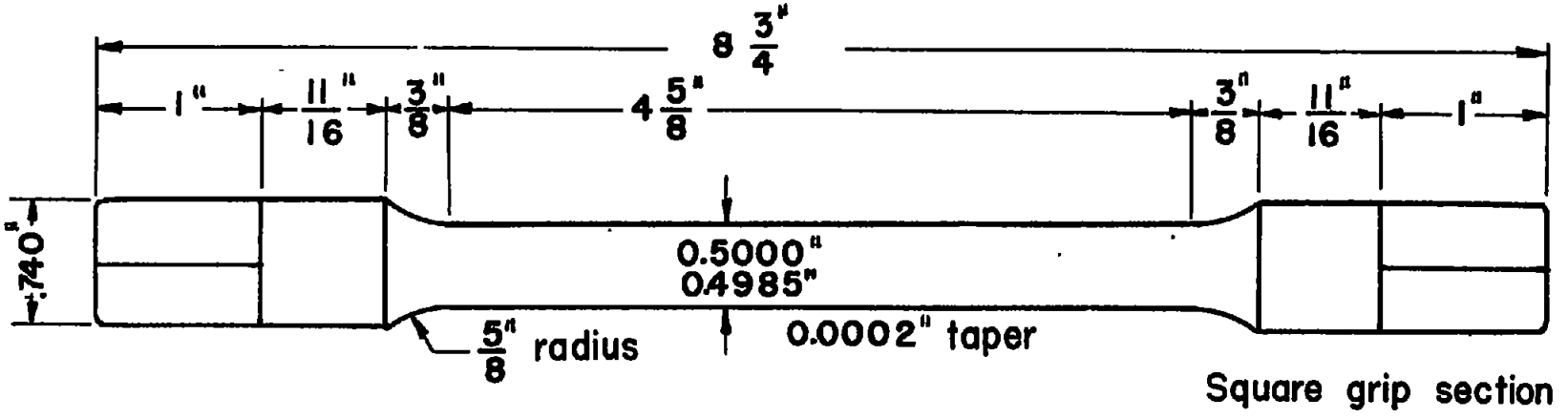

Figure 3.- Torsion test bar.

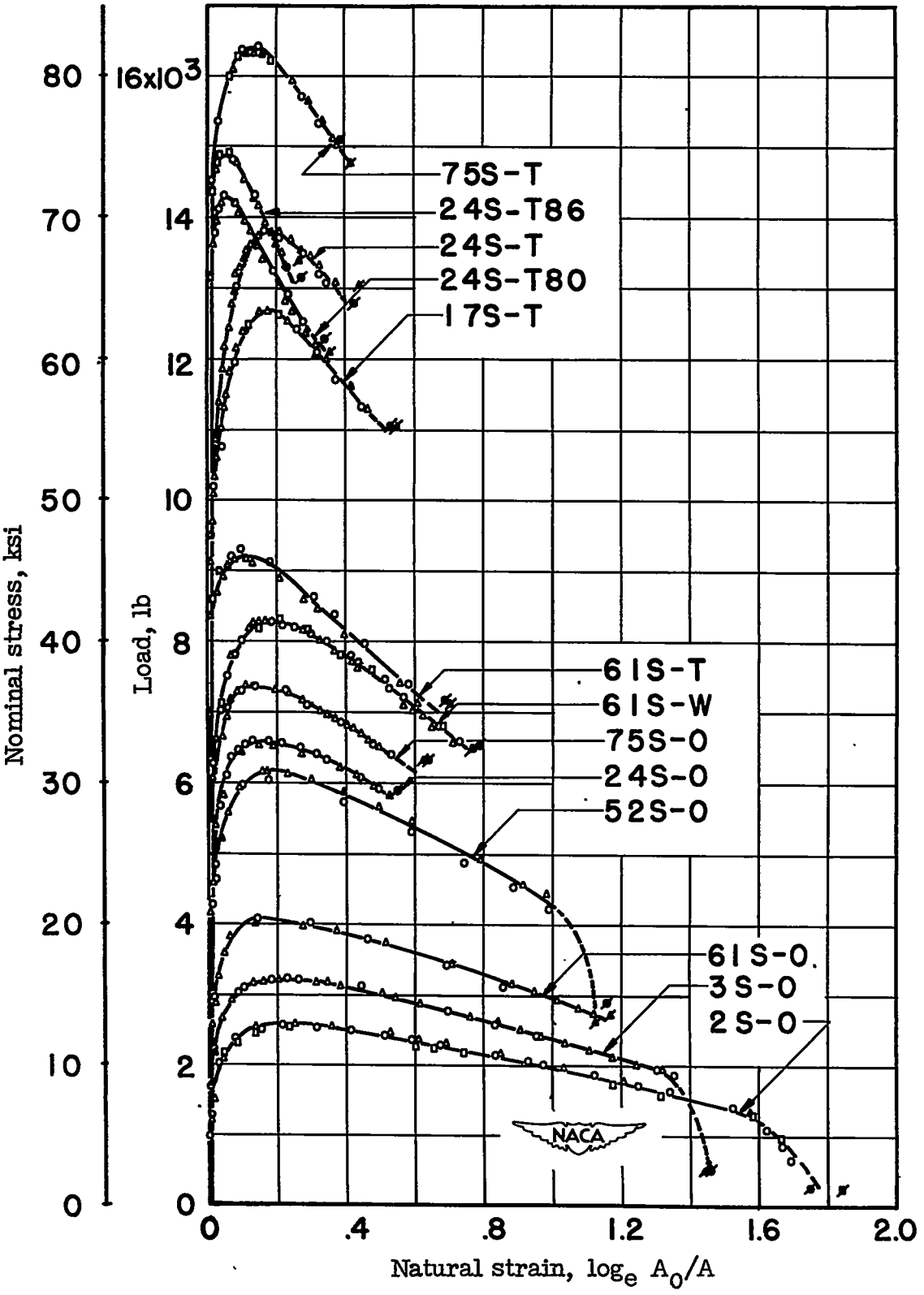

Figure 4.- Tension tests of various aluminum alloys.

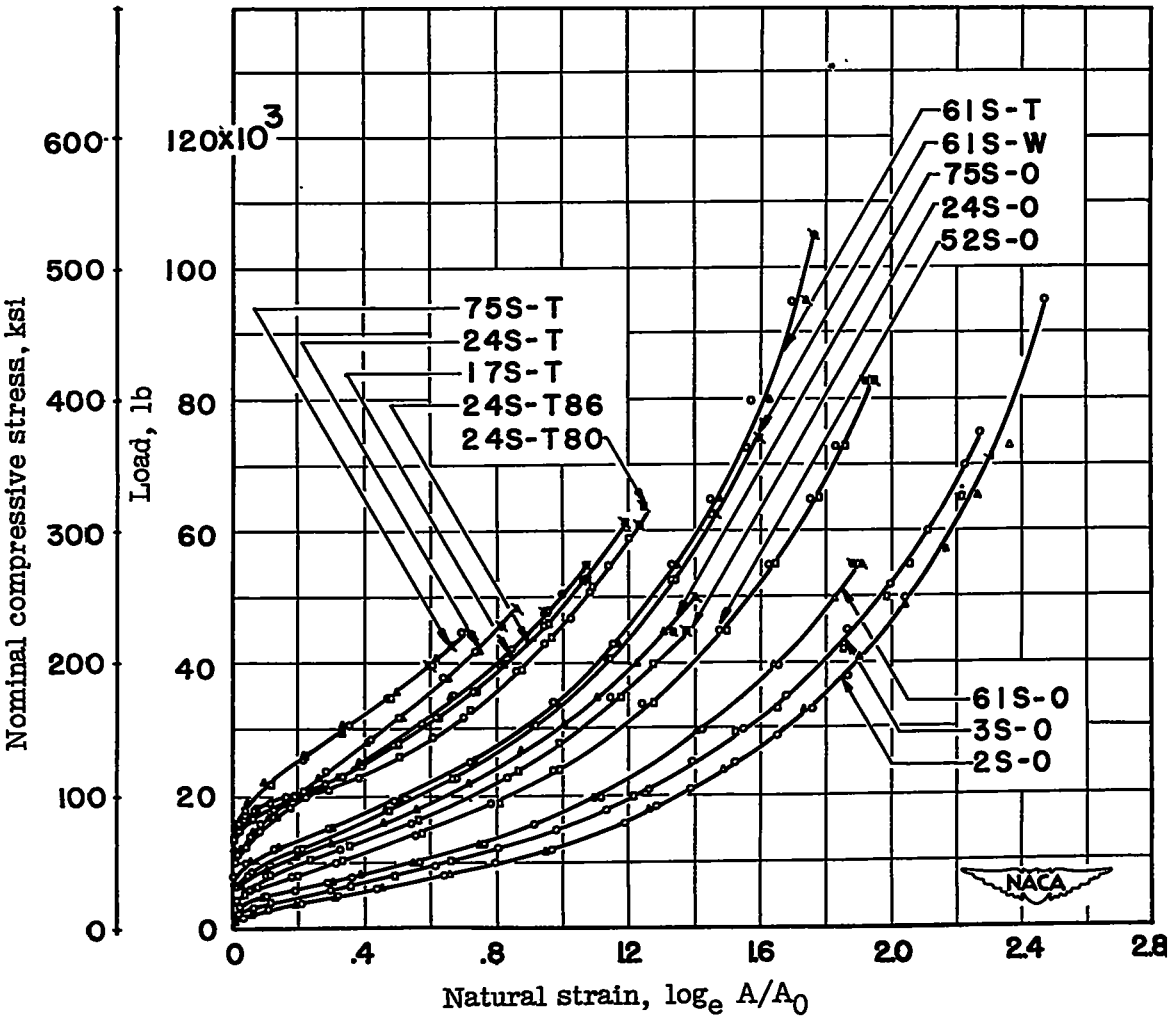

Figure 5.- Compression tests of various aluminum alloys.

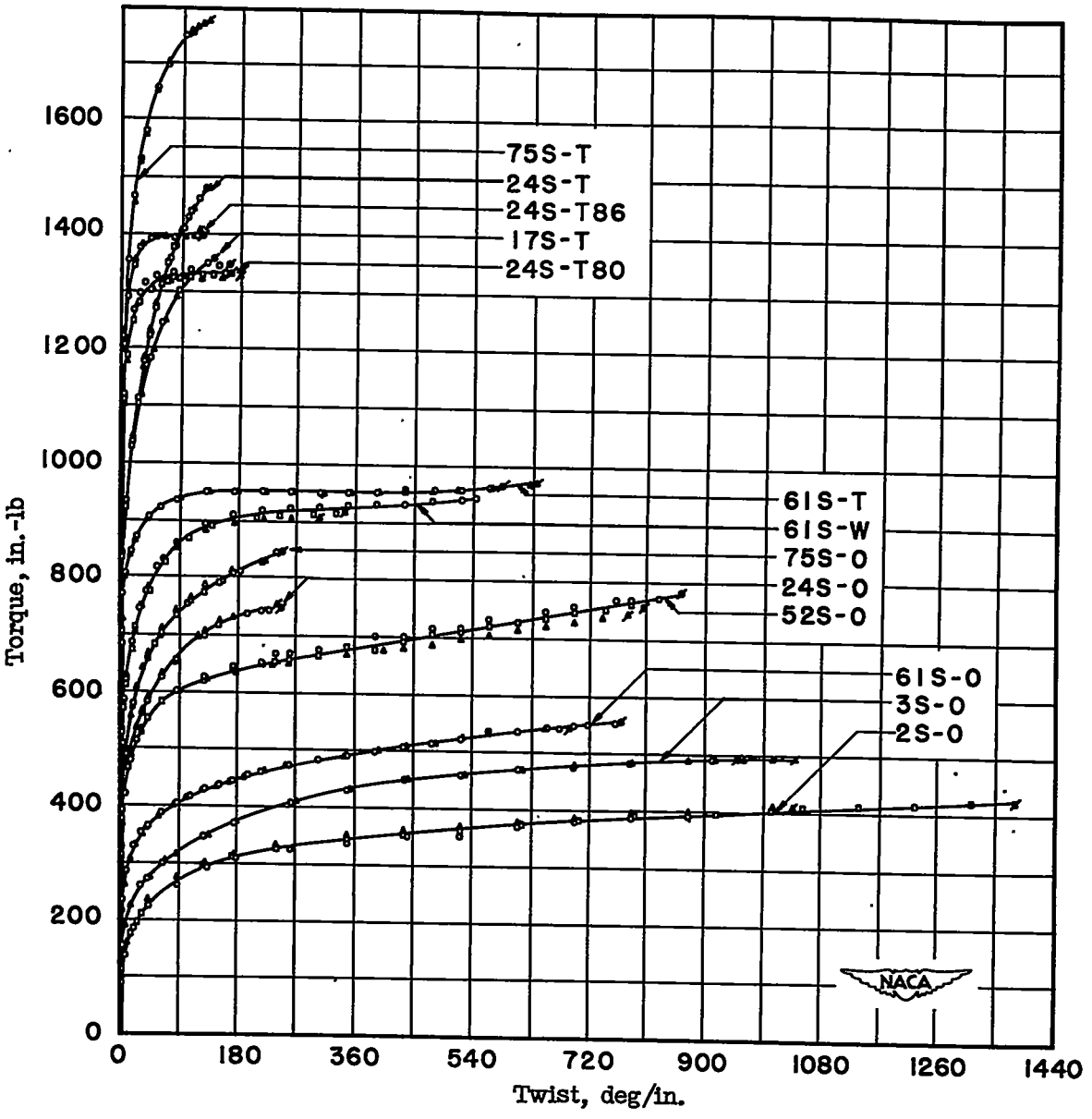

Figure 6.- Torsion tests of various aluminum alloys.

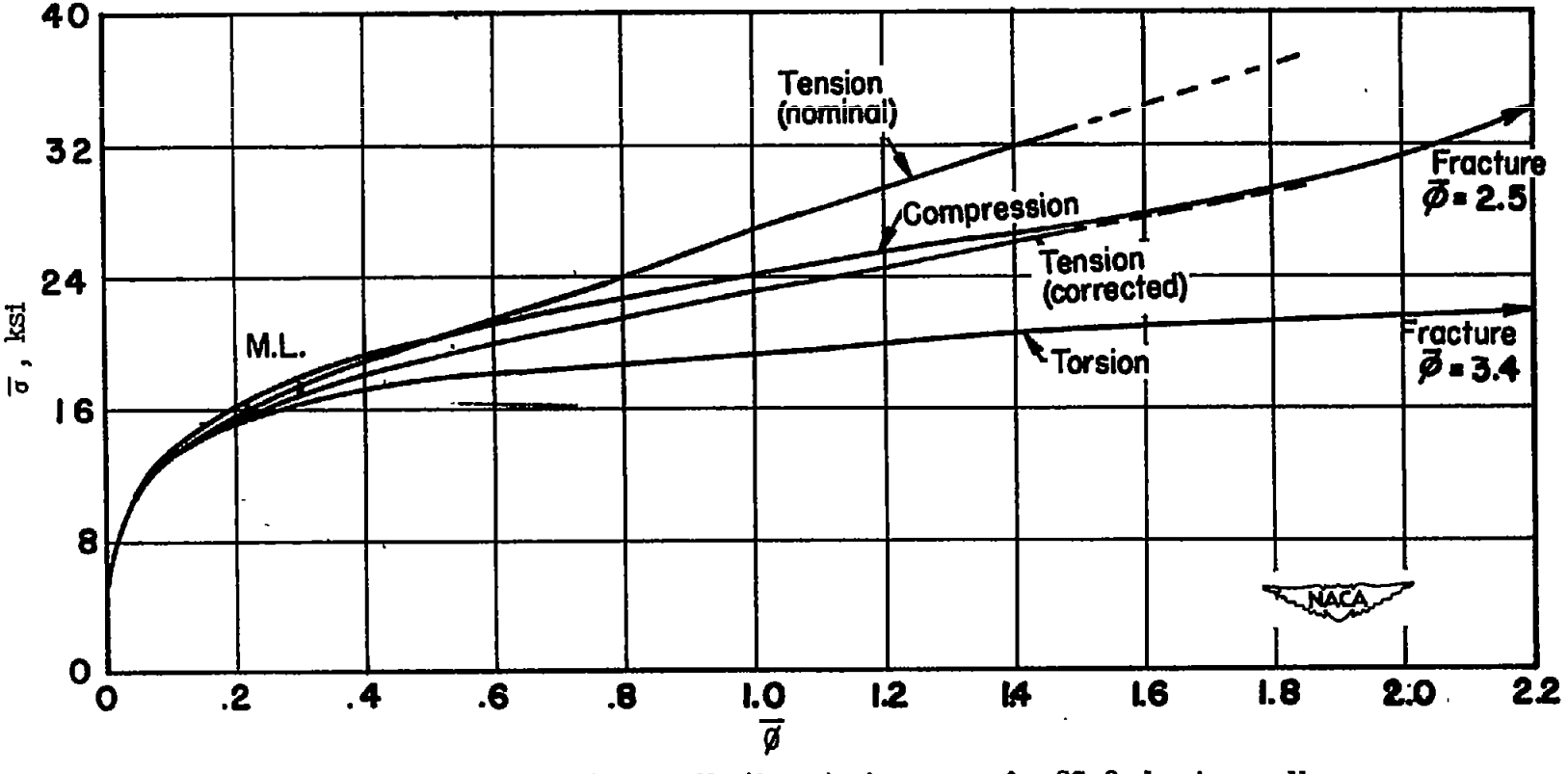

Figure 7.- Effective stress-effective strain curves for 2S-0 aluminum alloy.

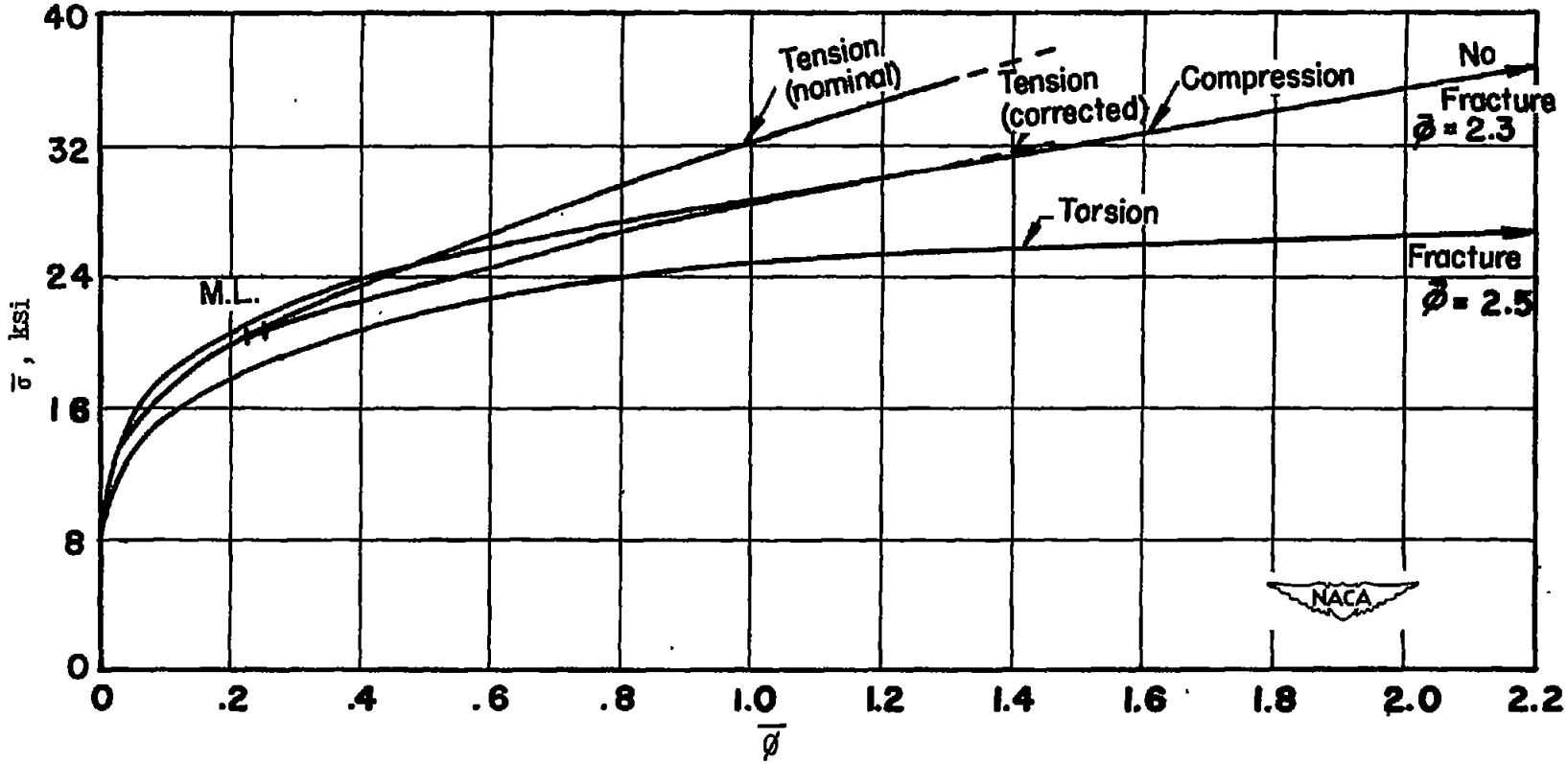

Figure 8.- Effective stress-effective strain curves for 3S-0 aluminum alloy.

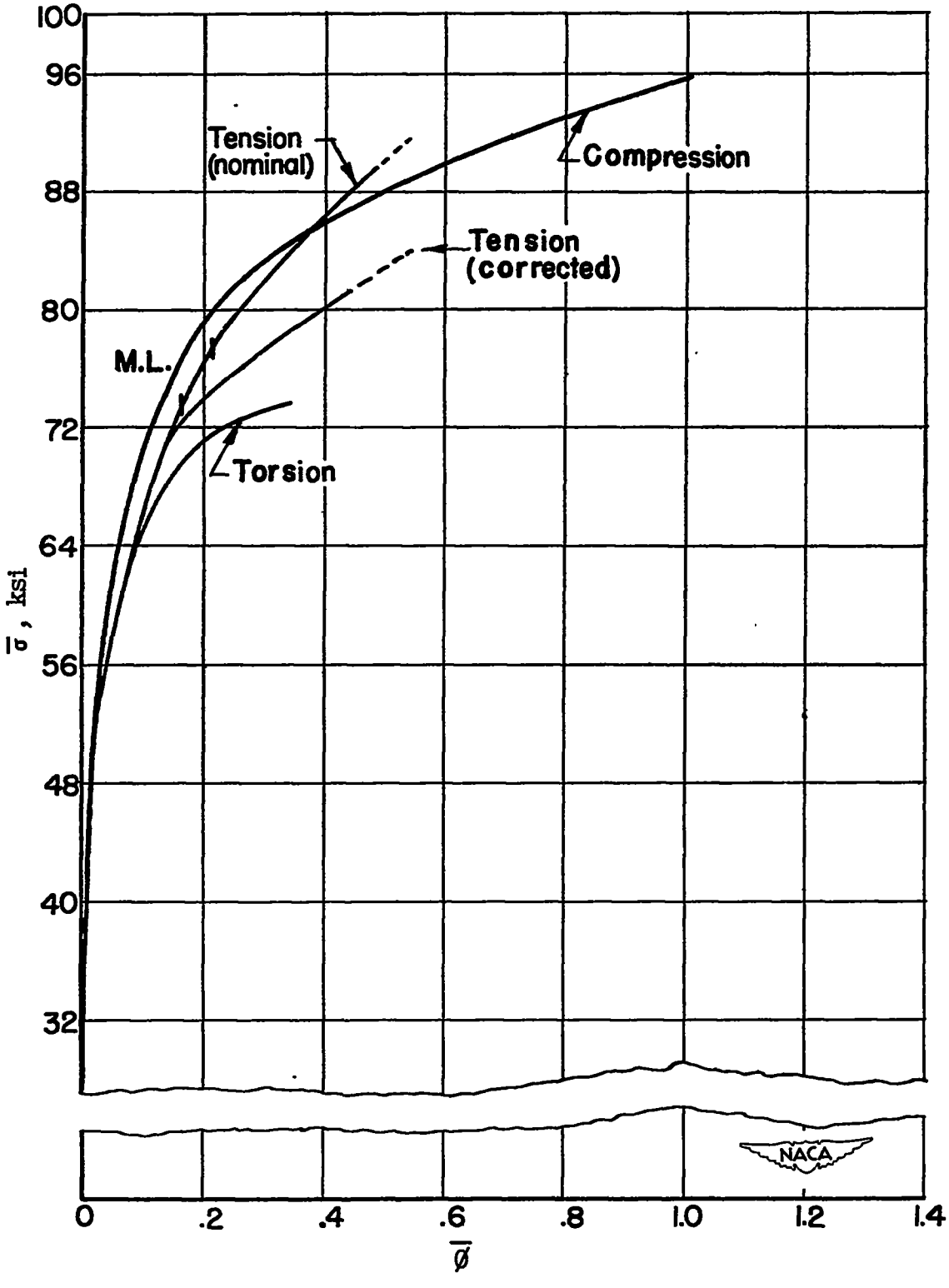

Figure 9.- Effective stress-effective strain curves for 17S-T aluminum alloy.

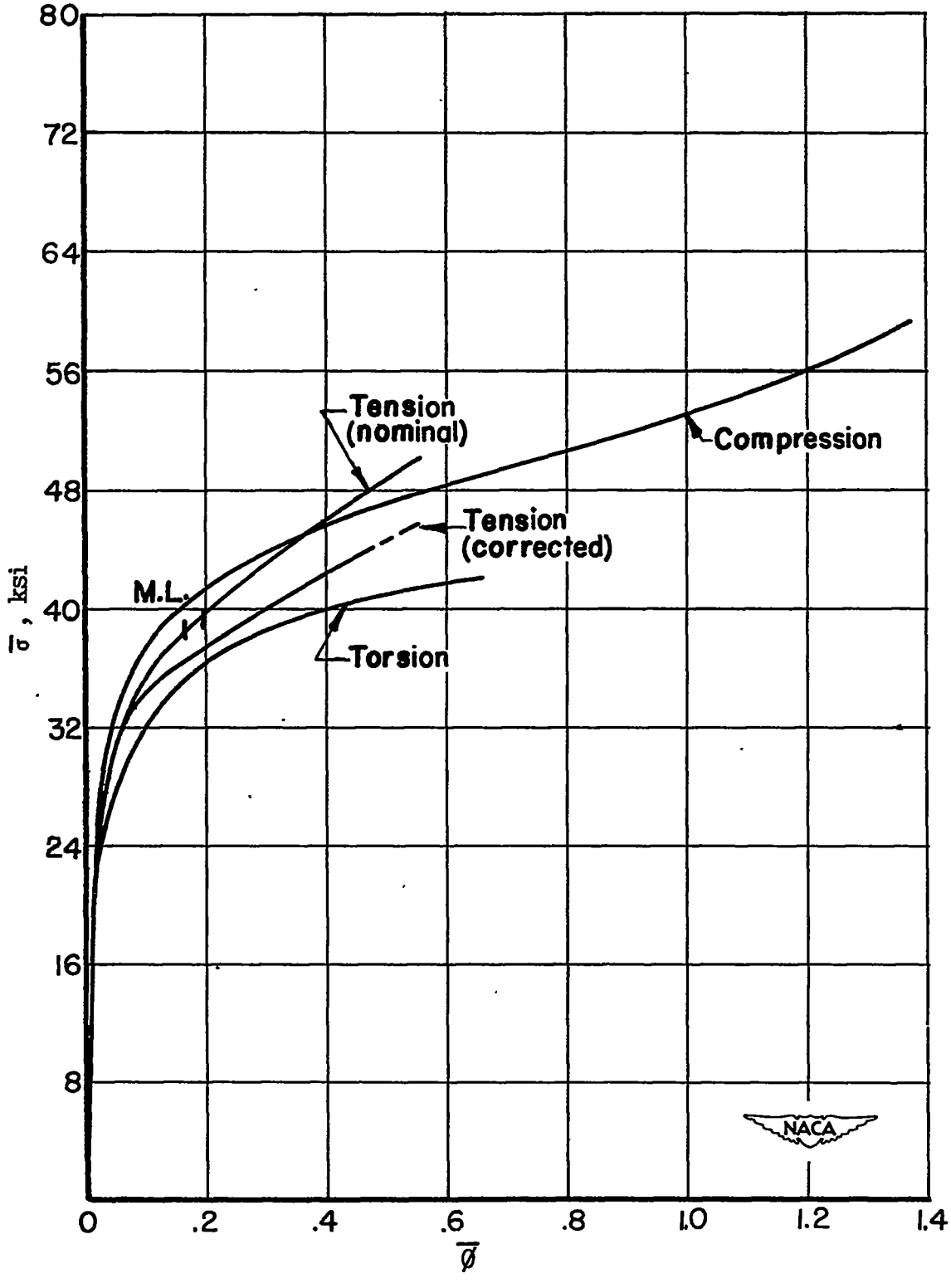

Figure 10.- Effective stress-effective strain curves for 24S-0 aluminum alloy.

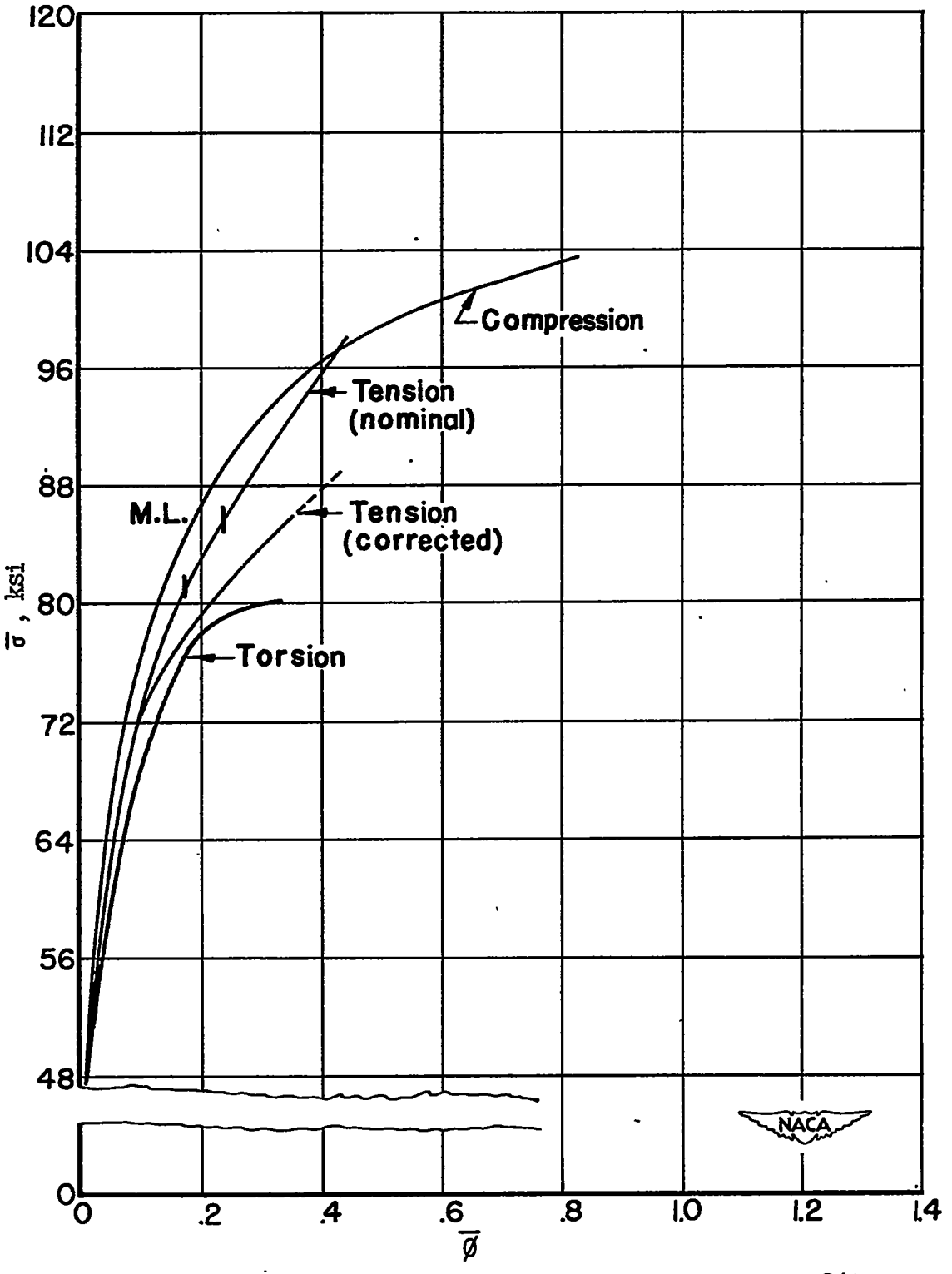

Figure 11.- Effective stress-effective strain curves for 24S-T aluminum alloy.

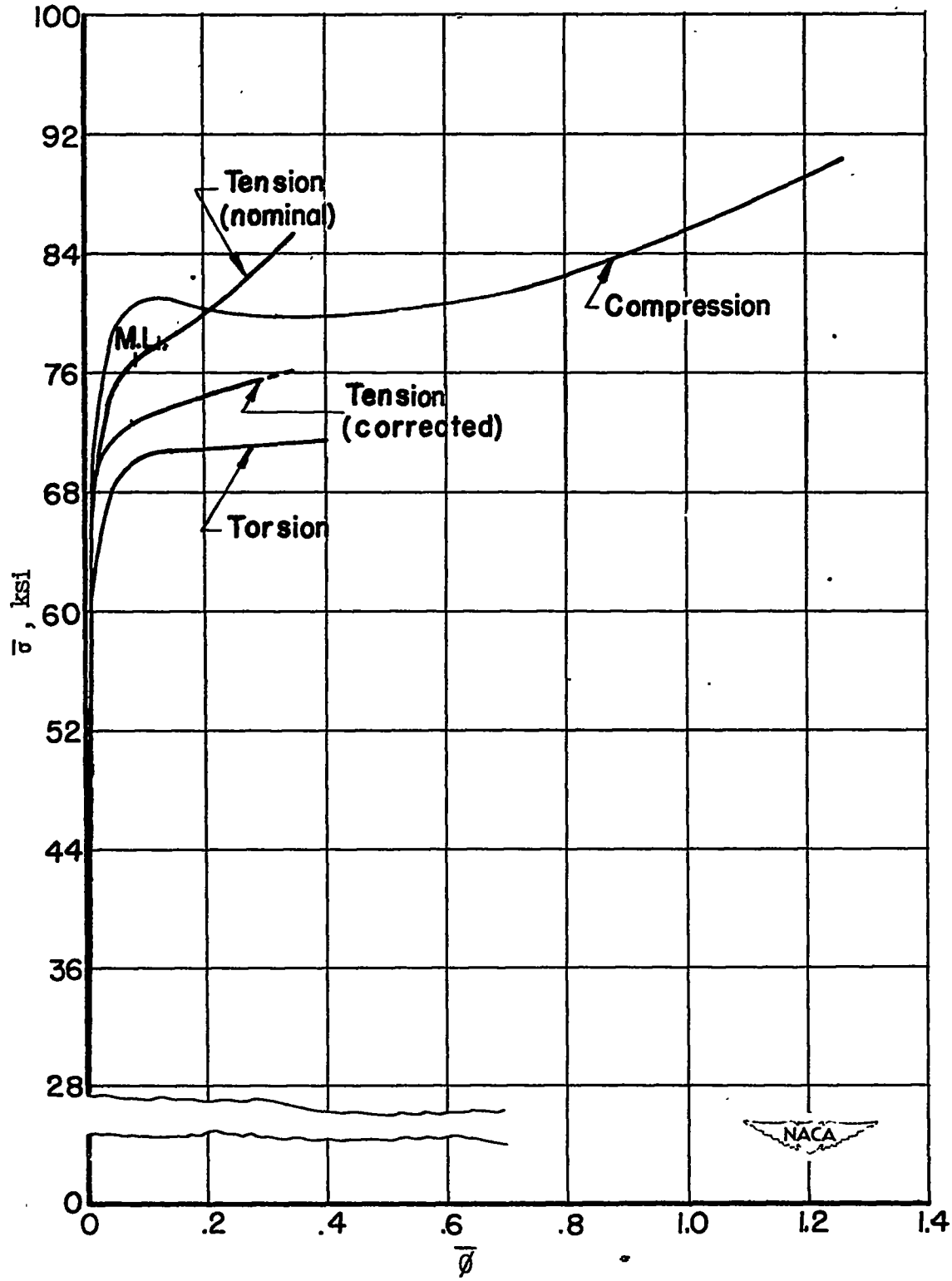

Figure 12.- Effective stress-effective strain curves for 24S-T80 aluminum alloy.

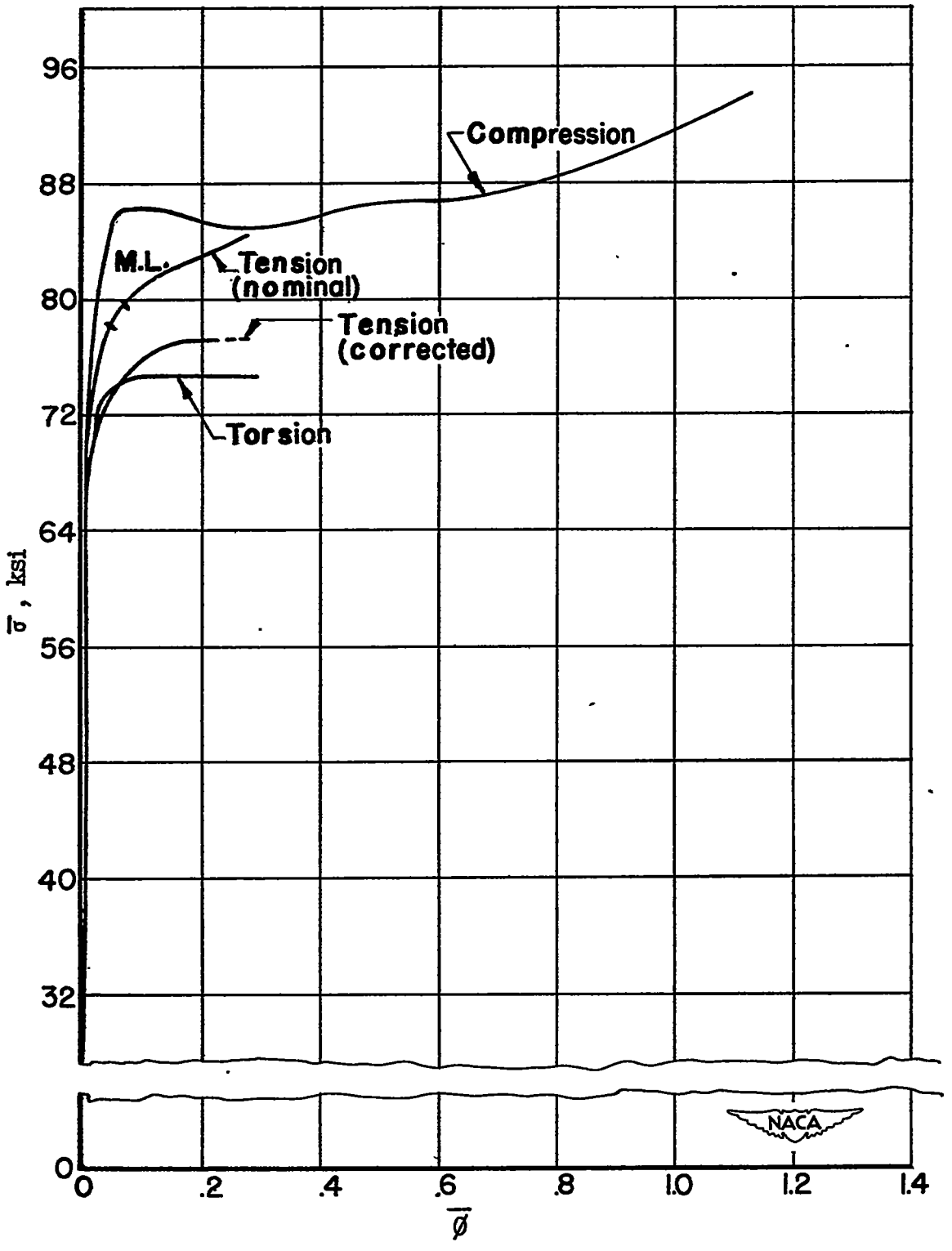

Figure 13.- Effective stress-effective strain curves for 24S-T86 aluminum alloy.

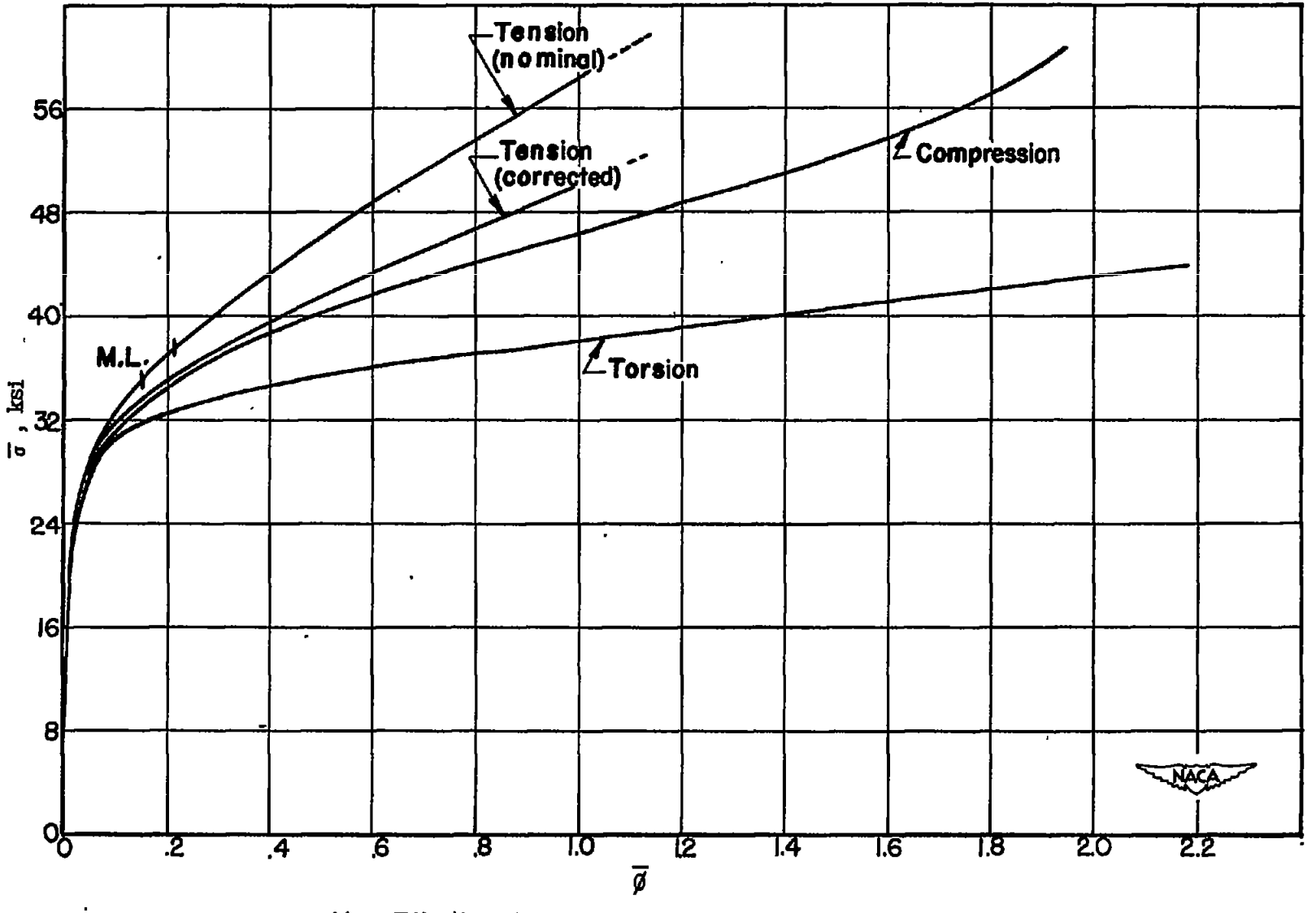

Figure 14.- Effective stress-effective strain curves for 52S-0 aluminum alloy.

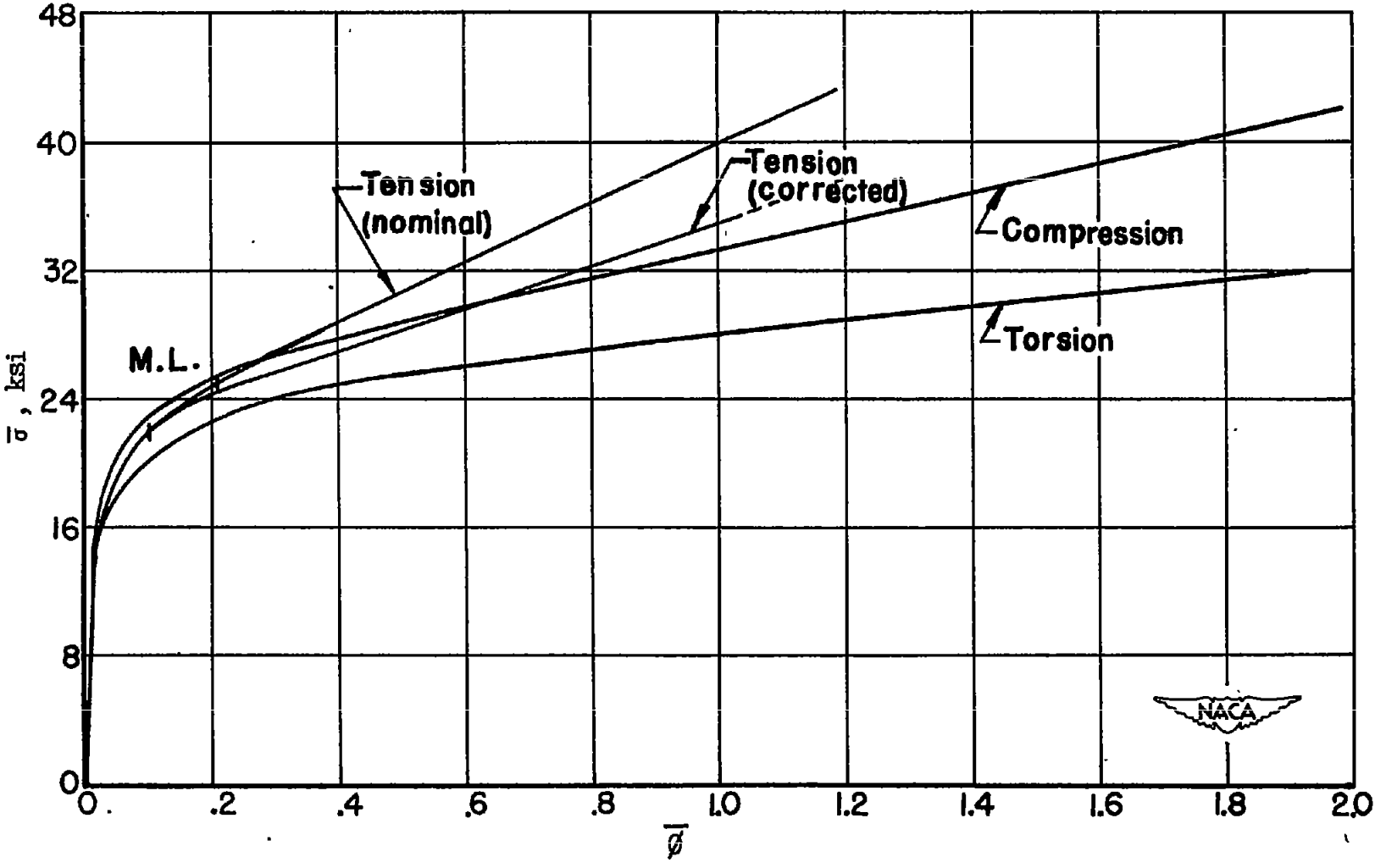

Figure 15.- Effective stress-effective strain curves for 61S-0 aluminum alloy.

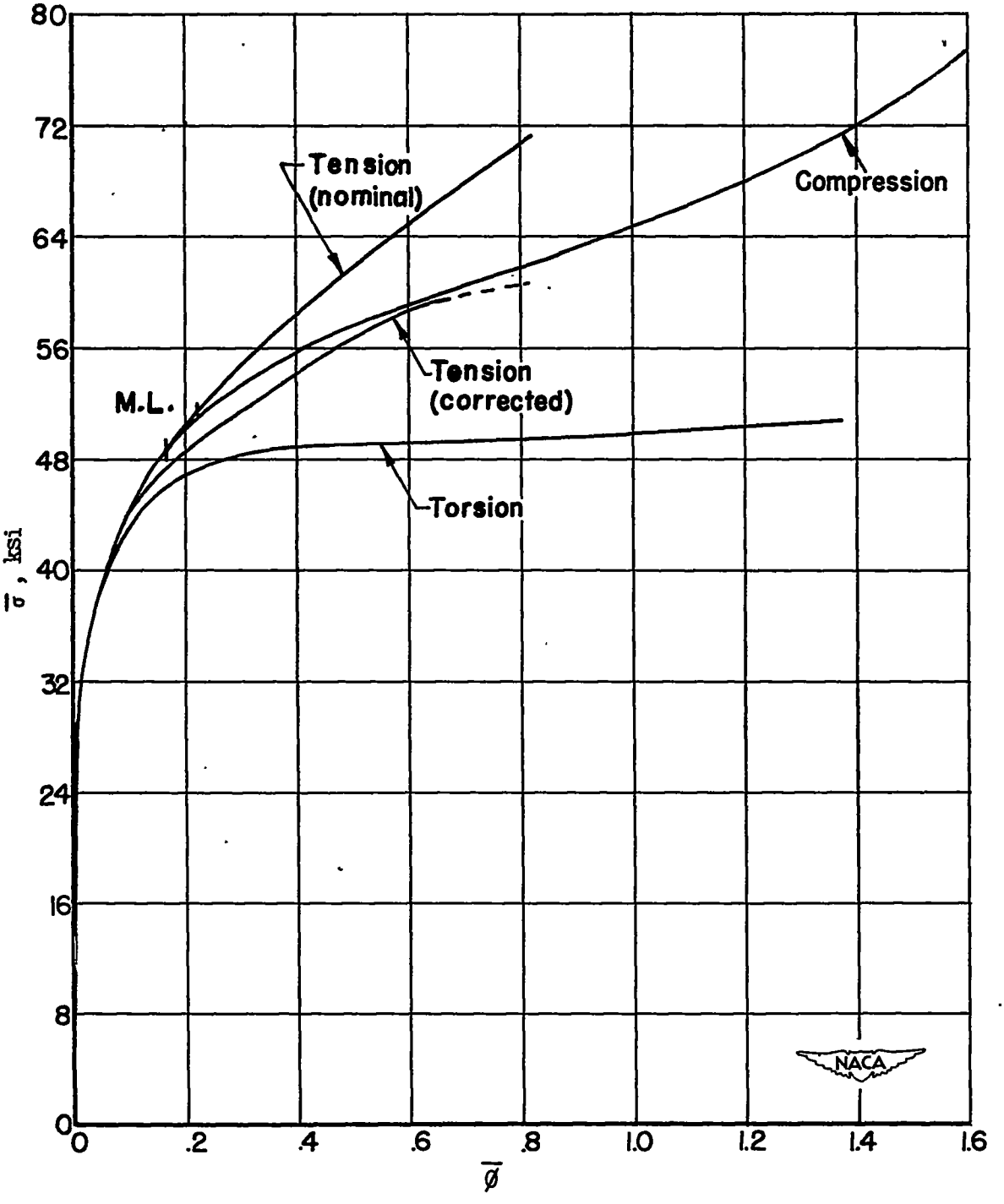

Figure 16.- Effective stress-effective strain curves for 61S-W aluminum alloy.

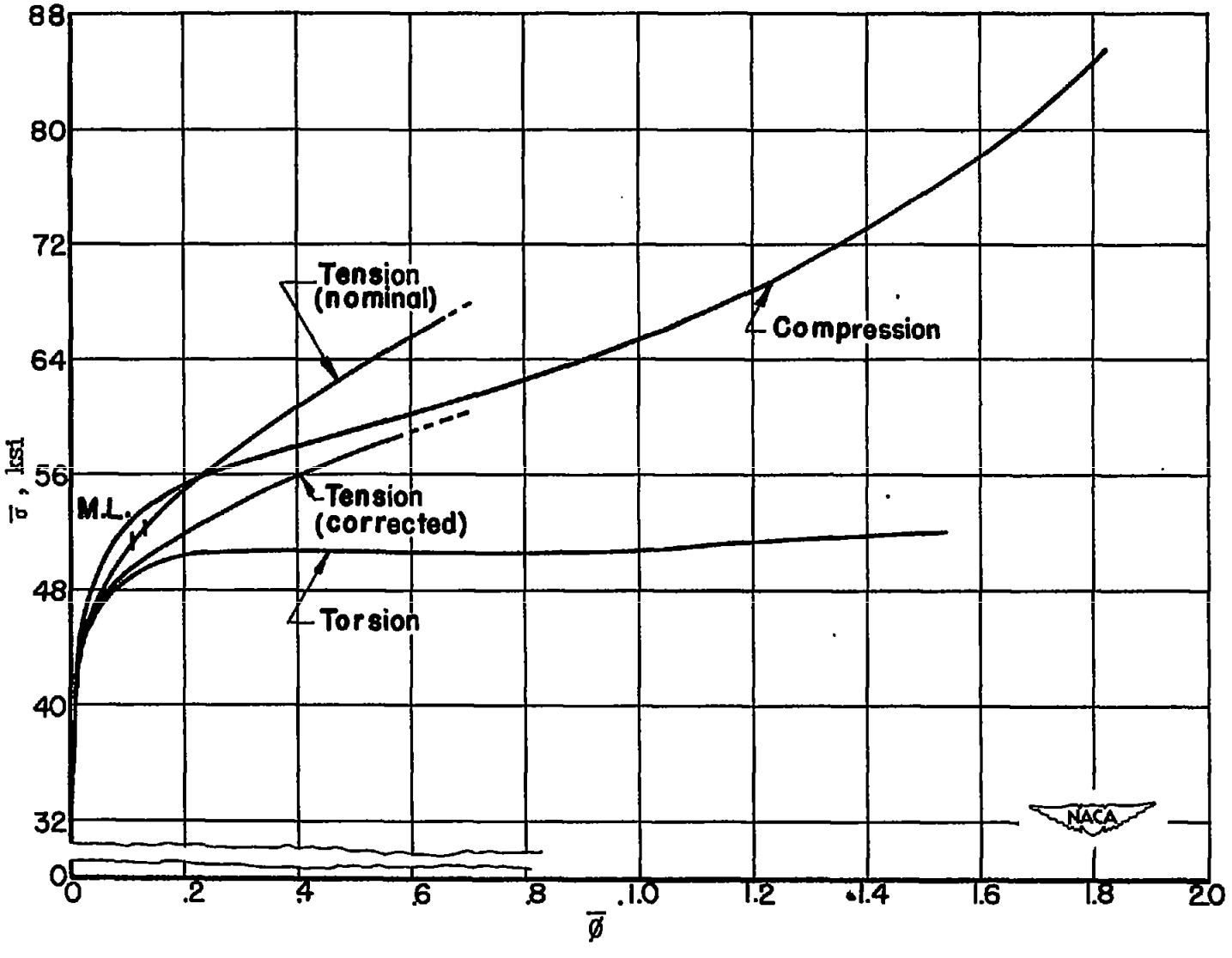

Figure 17.- Effective stress-effective strain curves for 61S-T aluminum alloy.

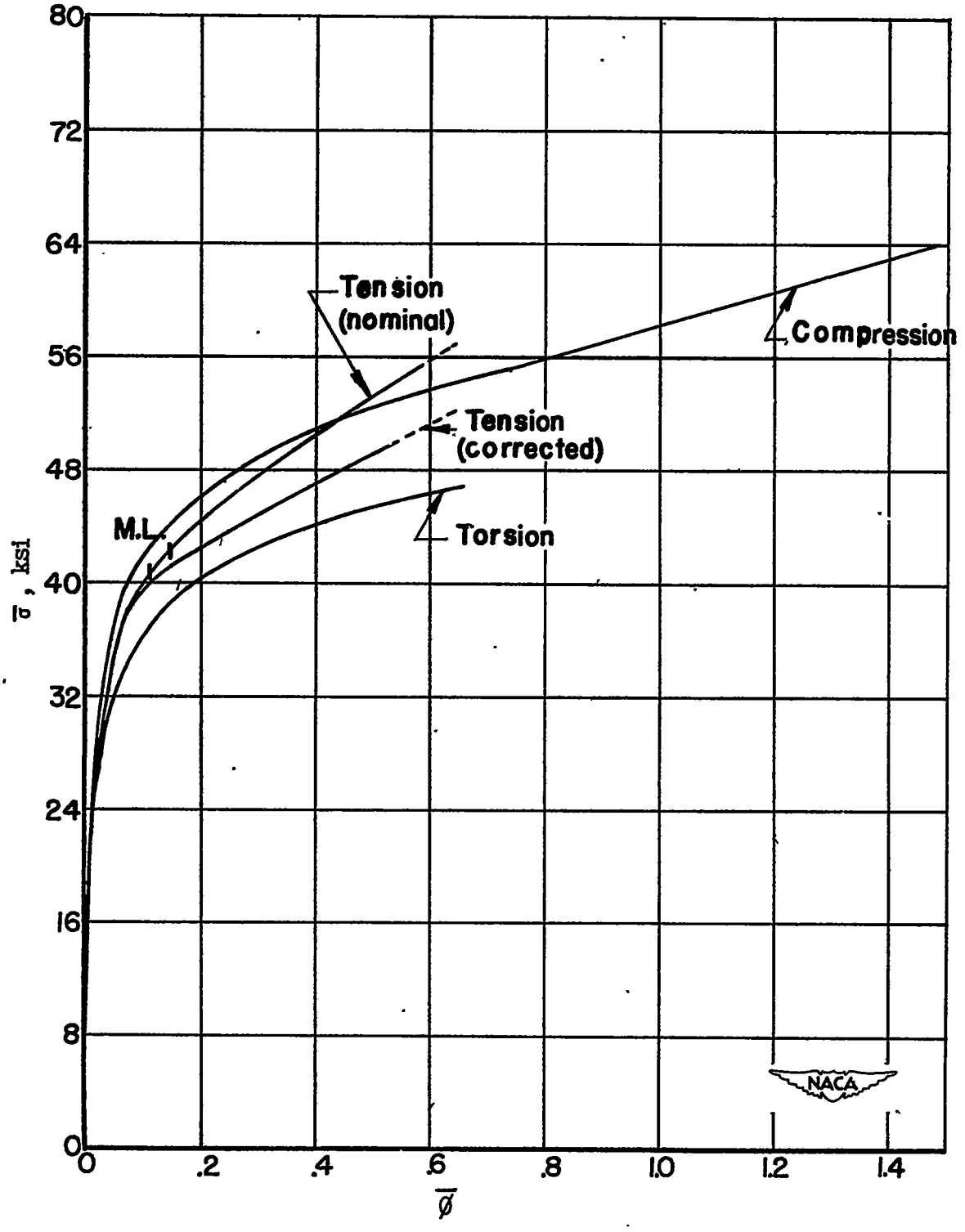

Figure 18.- Effective stress-effective strain curves for 75S-0 aluminum alloy.

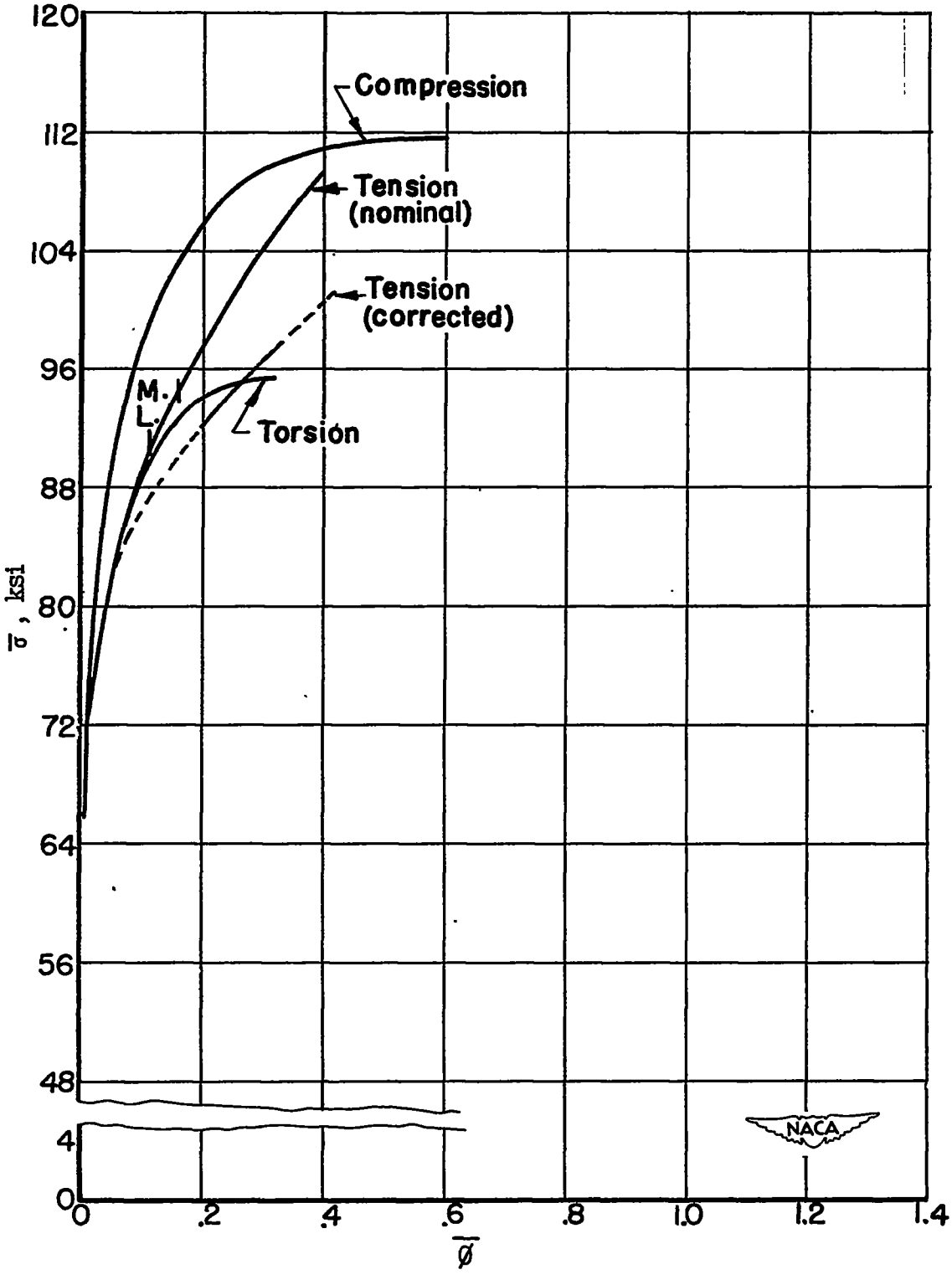

Figure 19.- Effective stress-effective strain curves for 75S-T aluminum alloy.

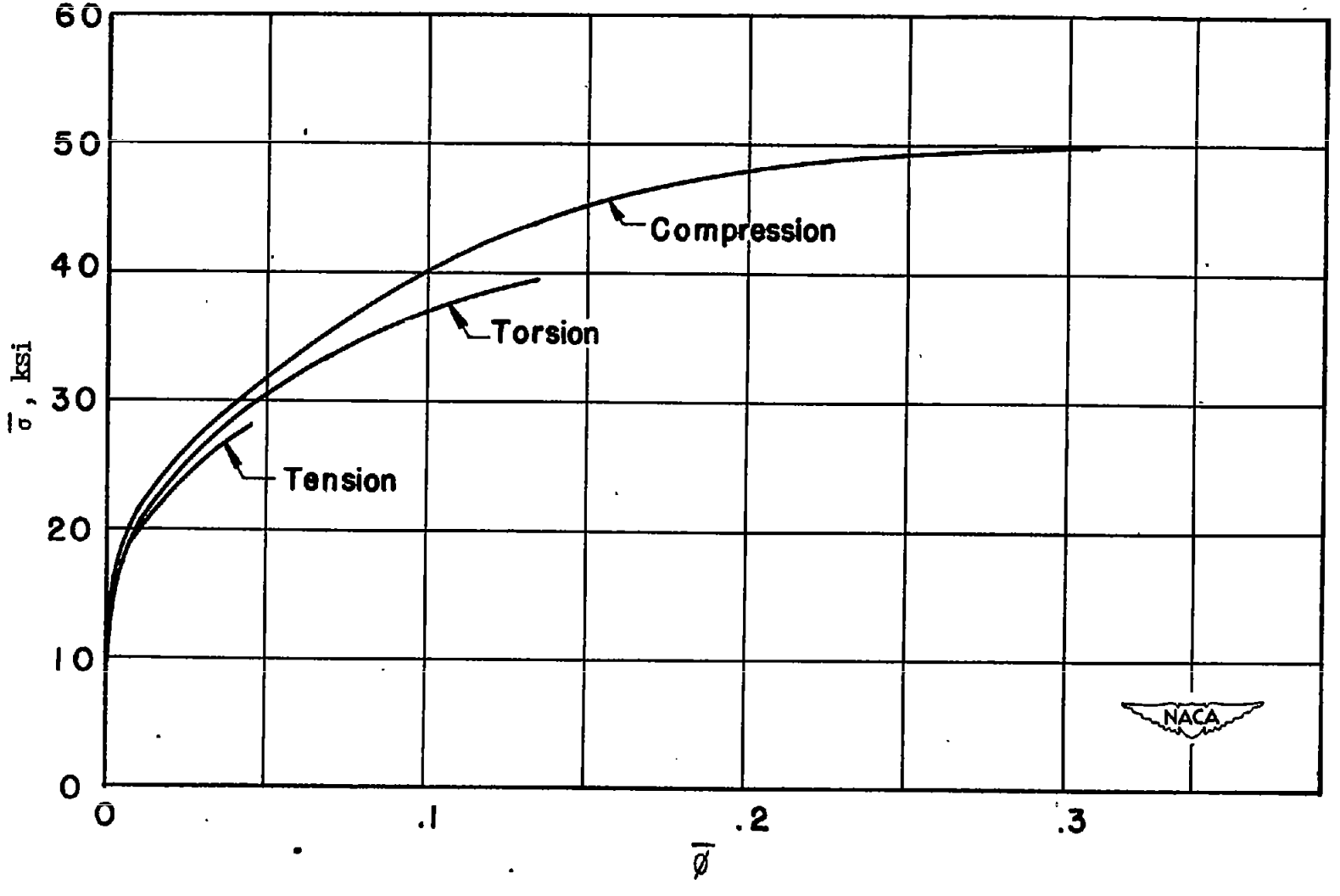

Figure 20.- Effective stress-effective strain curves for as-cast R magnesium alloy.

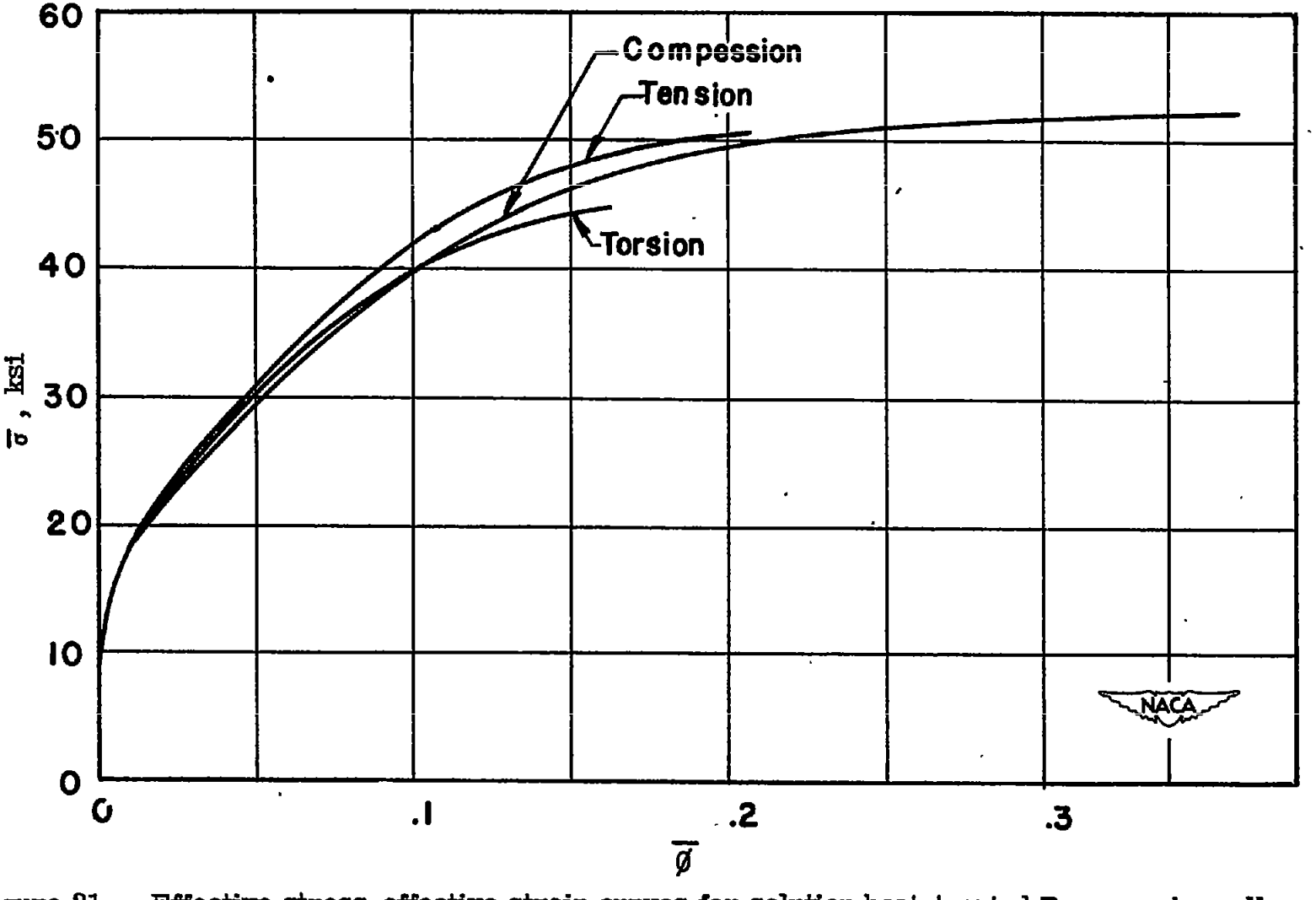

Figure 21.- Effective stress-effective strain curves for solution heat-treated R magnesium alloy.

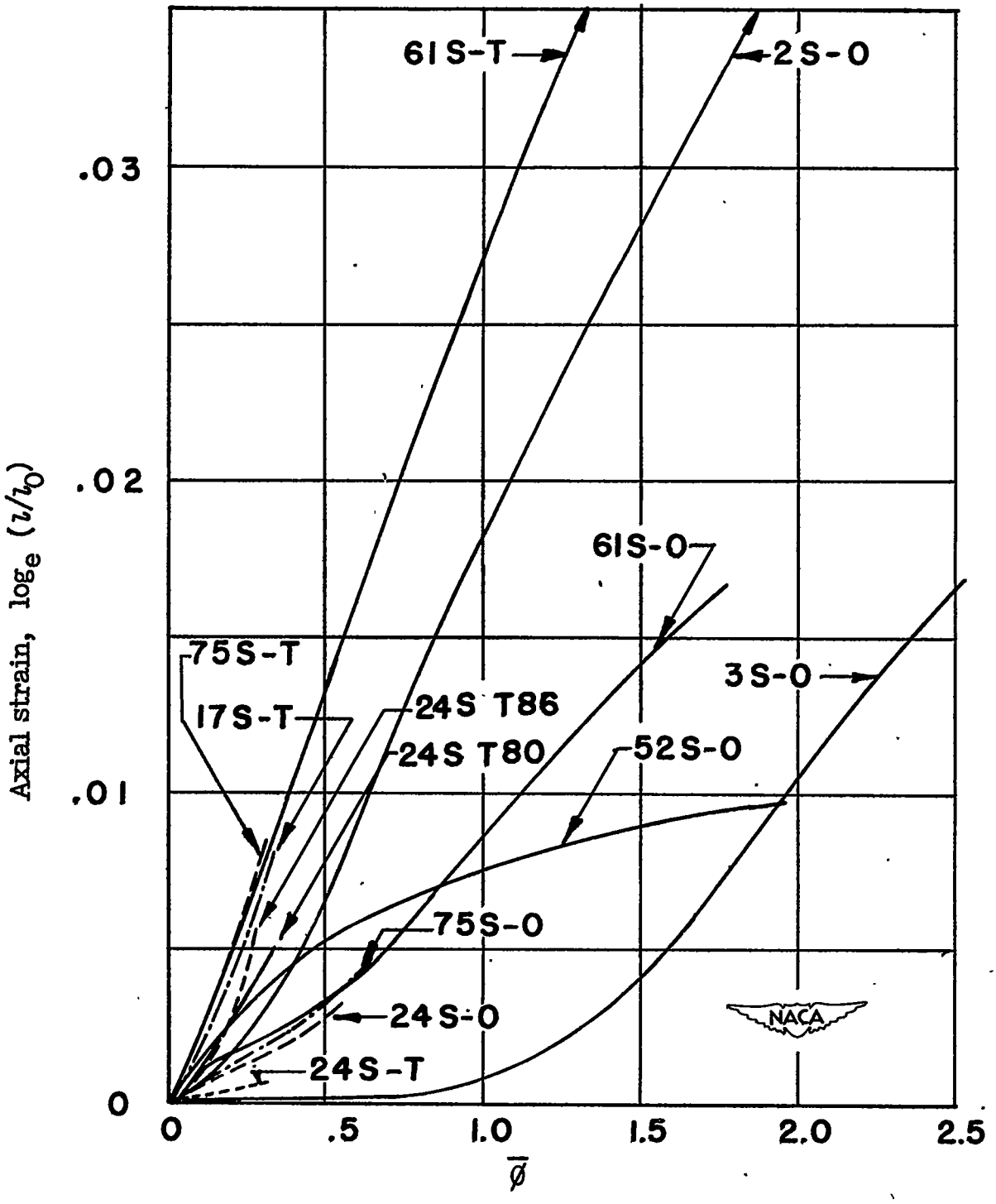

Figure 22.- Axial strain in aluminum-alloy torsion bars.

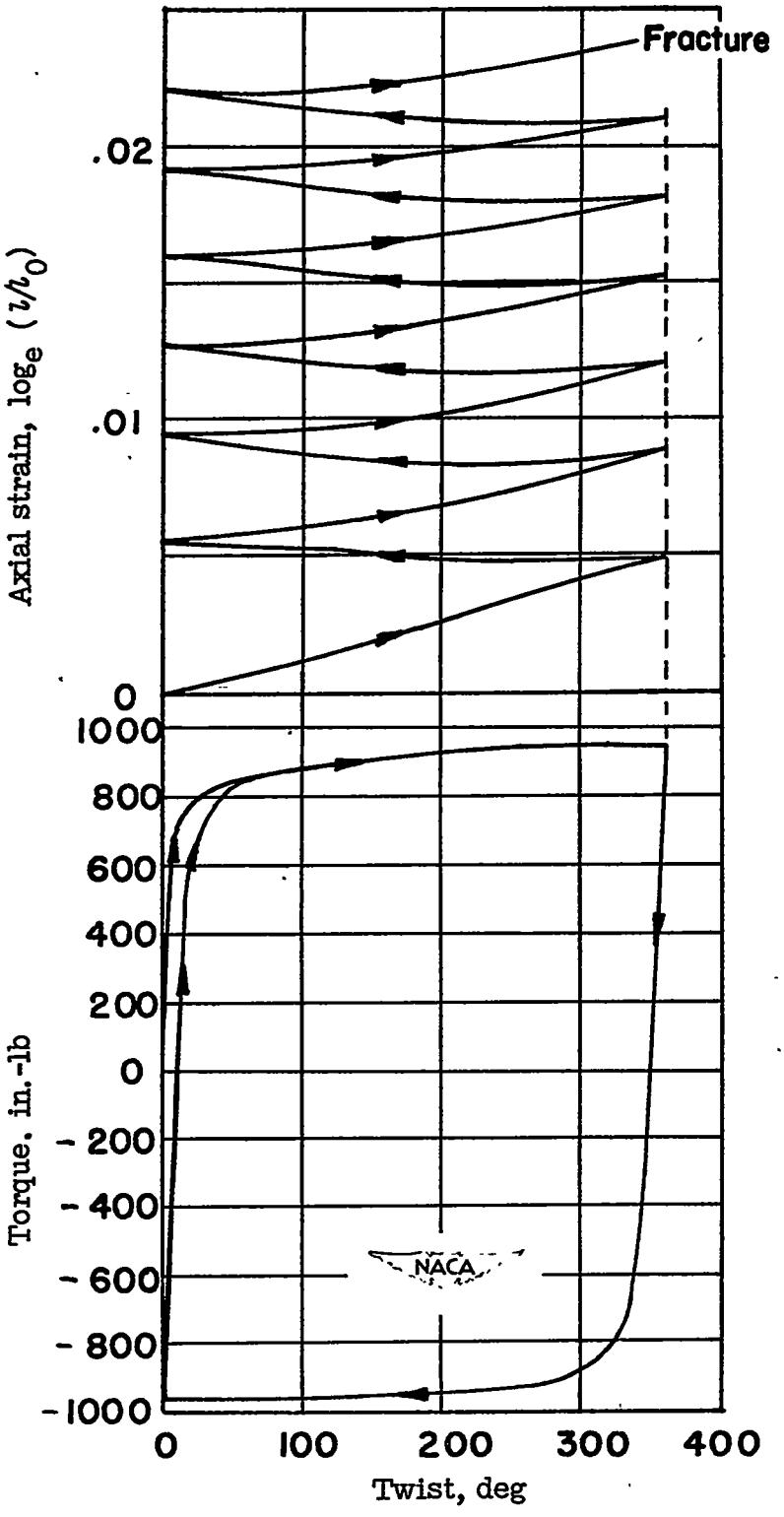

Figure 23.- Axial strain of 61S-T aluminum alloy subjected to reversal of torque.

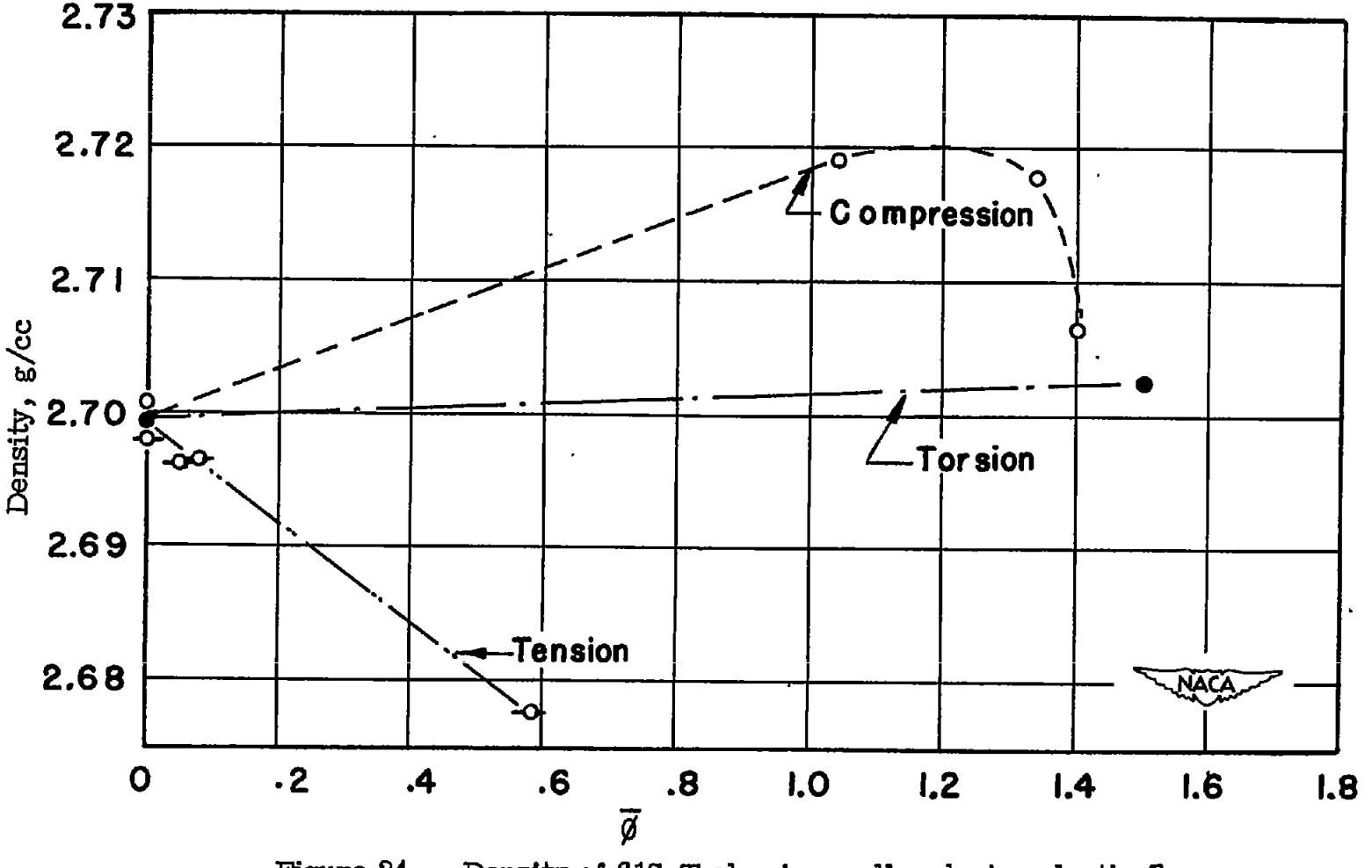

Figure 24.- Density of 61S-T aluminum alloy during plastic flow.